5-21-2004

Influence of Underfill on Ball Grid Array (BGA) Package Fatigue Life

Geetha Chilakamarthi
University of New Orleans

INFLUENCE OF UNDERFILL ON BALL GRID ARRAY (BGA) PACKAGE FATIGUE LIFE

A Thesis

Submitted to the Graduate Faculty of the
University of New Orleans
in partial fulfillment of the
requirements for the degree of

Master of Science
in
The Department of Mechanical Engineering

by

Geetha Chilakamarthi

B.Tech., Mechanical Engineering, J.N.T.University, India, 2000

May 2004

Acknowledgement

I would like to thank Dr. Melody Arthur Verges, my major professor, and my mentor for her sincere guidance, help, and giving me a chance to do this project. Without her, this would have been impossible.

I am grateful to Dr. Paul D. Schilling and Dr. Paul D. Herrington for serving on my graduate committee.

Furthermore, I would like to thank all the people that have helped and encouraged me in completing this work: my parents, Bhanu Prasad, Vijaya Lakshmi, my sister Sandhya, and my friend Nelson Akafuah who provided inspiration and support when needed.

Finally, I would like to acknowledge Jesus Christ. Since coming to know Him, my life has never been the same. He has transformed me emotionally and spiritually and to Him I give glory. I like to finish my acknowledgement with one of my favorite Bible verses:

Philippians 3:12-14 “Not that I have already obtained all this, or have already been made perfect, but I press on to take hold of that for which Christ Jesus took hold of me. I do not consider myself yet to have taken hold of it. But one thing I do: Forgetting what is behind and straining toward what is ahead, I press on toward the goal to win the prize for which God has called me heavenward in Christ Jesus”.

Dedication

I dedicate this project to my parents, who have provided me with support emotionally and financially throughout this long journey called my college career, and to Ratan, my greatest emotional and spiritual support. He continuously encouraged me, prayed for me and patiently stood by my side. I thank God for the rest of my family, who supported me with their prayers and encouraging words.

I thank Jesus Christ, my Savior, for His unconditional love, forgiveness, patience, grace and mercy.

TABLE OF CONTENTS

List of Figures v

Abstract vii

1. Introduction 1

2. Literature Review 6

2.1 Basic Fatigue Life Approaches 6

2.2 Fatigue Life of Solder connections 9

2.3 Fracture Model for Solder connections 11

3. Finite Element Model 15

3.1 Finite Element Geometry 16

3.2 Boundary Conditions 17

3.3 Material Constituents 19

3.4 Thermal Loading 20

3.5 Convergence Criterion 21

4. Results 24

4.1 Influence of Underfill Parameters 25

4.2 Significance of Mode I Cyclic Stresses 30

4.3 Comparison of Mode I Cyclic Stresses with Mode II Cyclic Stresses 37

5. Conclusions and Recommendations 40

References 42

Appendix A 44

Appendix B 47

Vita 53

List of Figures

Figure 1.1(a) Picture showing top view of BGA package 2

Figure 1.1(b) Picture showing side view of BGA package 2

Figure1.2 Schematic of row of interconnects subjected to thermal cycling (a) The shape of interconnects at some reference temperature T (b) Deformed shape of interconnects at some maximum temperature T_1 (c) Deformed shape of interconnects at some minimum temperature T_0 4

Figure 1.3 Schematic showing the crack prone areas in the solder 4

Figure 2.1 The three types of loading that can be experienced by a crack 8

Figure 2.2 Schematic depicting stresses on an edge crack. (a) Mode II shear stress. (b) Shear stress with an additional compressive Mode I stress. (c) Shear stress with an additional tensile Mode I stress 12

Figure 3.1 A three dimensional view of a unit cell. The inner cylinder is representative of the solder connection while the outer cylinder is representative of the underfill 15

Figure 3.2(a) Three-dimensional view of the unit cell with a highlighted section showing the cross-sectional view of the finite element geometry 17

Figure 3.2(b) Two dimensional geometry used in the creation of the axisymmetric finite element model 17

Figure 3.3 Schematic of finite element geometry with the dimensions and boundary conditions 19

Figure 3.4 Ansys plot showing the mesh of finite element geometry 22

Figure 3.5 Graph depicting the convergence criterion for normal stress values along the top boundary of the solder interconnection. The underfill material properties for this case E_u=3.5GPa, ν_u=0.3, and α_u=100X10^{-6}/K. The temperature loading is from 25°C to 5°C 23

Figure 4.1 Graph depicting normal stress values along the top boundary of the solder interconnection. The underfill properties for this case are E_u=3.5GPa, ν_u=0.3, and α_u= 100x10^{-6}/K. The temperature loading is from 25°C to 5°C 25

Figure 4.2 Graphs depicting the normal stresses at the nodes located at the middle of the solder interconnect (a)E_u=2.0GPa (b)E_u=3.5GPa (c)E_u=5.0GPa (d) E_u=6.5GPa (e) E_u=8.0GPa.....26

Figure 4.3 Schematic of the fluctuation of normal stresses over a temperature cycle for the case of E_u=2.0GPa and ν_u=0.3 assuming temperature profile is sinusoidal (a) α_u=10x10^{-6}/K (b) α_u=40x10^{-6}/K (c) α_u=70x10^{-6}/K (d) α_u=100x10^{-6}/K 29

Figure 4.4 Schematic showing the addition of Mode I cyclic stresses to steady state stresses 31

Figure 4.5 Graphs depicting the most tensile stresses induced in the solder during one thermal cycle when temperature is 5°C and *%sh* of underfill material is 0.6 (a) E_u=2.0GPa (b) E_u=3.5GPa (c) E_u=5.0GPa (d) E_u=6.5GPa (e) E_u=8.0GPa 32

Figure 4.6 Plot depicting the normal stresses for the case when $\nu_u = \nu_s$ and $\alpha_u = \alpha_s$ 35

Figure 4.7 Graph depicting the normal stress values for real underfill material properties....36

Figure 4.8 Schematic of sinusoidal plot of Mode I stresses for real underfill material properties.....37

Figure 4.9 Schematic of top view of a ten by ten array of solder interconnects in BGA package (the numbered joints represents the joints for which shear stress is calculated).....38

Abstract

The influence of underfill material properties on the fatigue life of Ball Grid Array (BGA) packages that are subjected to thermal cycling is investigated in this study. A finite element model is created using *Ansys* by assuming the existence of an infinite array of solder interconnects, cylindrical in shape, surrounded by underfill material. Axial stresses in the interconnects are determined as a temperature loading is applied. The results show that these normal stresses are on the same order of magnitude as the hydrostatic compressive stresses induced in the solder upon underfill curing. Therefore it is concluded that for the range of underfill properties tested, these Mode I cyclic stresses need to be considered in the development of a fracture-based fatigue life model. In addition, a guideline is provided to aide researchers in designing experiments that will replicate loads on fractured specimens that are consistent with those seen in aerospace applications.

1. Introduction

The rapid improvement in the electronic industry across a wide range of sectors including aerospace and automotive, are dependent on the structural integrity of embedded micro-electronic components and assemblies. Solder joints were initially intended to be simple electrical interconnections between mechanically interlocked components in electronic packages. However, as with any new technology, the size of electronic components have been decreasing while the number of input/output terminations have been increasing. As a result, the number of solder joint connections have increased while the dimensions of joint have decreased. Moreover, packaging engineers are interested in incorporating even smaller solder joints as the need increases for designing packages with more performance options. Several packaging technologies have emerged in which area array packages, namely Ball Grid Array packages (BGA) and peripheral packages, namely Quad Flat Packages (QFP), have become more popular. The BGA package offers double the package pin count when compared with QFP package. In addition, BGA packages provide better package performance and manufacturing yield than QFP packages. Hence the BGA package has become more prevalent among electronic packages. A typical BGA package is shown in Figure 1.1(a). As shown in Figure 1.1(b), a BGA package is composed of three basic parts:

1. Chip Carrier
2. Printed Circuit Board (PCB)
3. Solder Interconnect

(a)

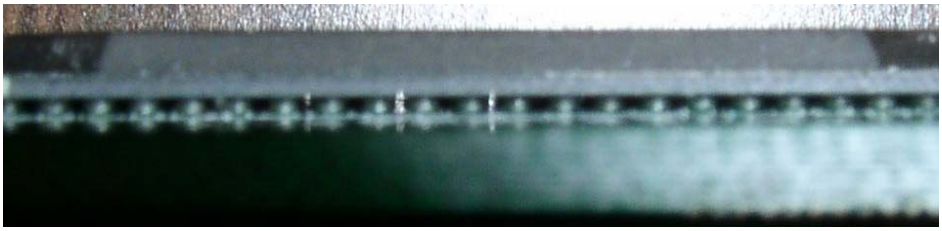

(b)

Figure 1.1 Picture of the BGA package. The top component is the integrated circuit chip. The bottom component is the printed circuit board. (a) Top view of package. (b) Side view of package.

The solder interconnects are joined to the respective integrated chip carrier and PCB. There are various techniques used to apply solder on to component or board metallizations such as electroplating, solder preforms, and solder paste. When solder preform or solder paste is used, flux is usually included to remove surface oxides and promote wetting and spreading of reflowed solder. Solder preform is just a small mass of solder alloy which is in the shape of a cylinder,

disc, sphere etc. which contain flux as an inner core. The solder paste is actually a suspension of solder particles in a cream flux. The additives are included in the cream flux to promote wetting and control paste properties. Generally solder paste is applied to the metallizations on the PCB using a screen printing or stencil operation Once the paste is applied to the circuit board, the components are usually positioned on the board and held there by the tackiness of the paste. This package is then 'reflowed' in an oven, or some other heating mechanism, so that the joints are formed [Frear et.al, (1994)].

The reliability of solder joints is one of the critical issues in surface mount technology. A key issue in long term reliability of solder joints is joint failure during thermal cycling. The individual components that are soldered together in an electronic package typically have different thermal expansion coefficients. When this package is subjected to a thermal loading, the interconnects undergo shear as a result of a mismatch of coefficient of thermal expansion between the chip carrier and the PCB. If, for example, the coefficient of thermal expansion of the chip is greater than that of PCB, the chip carrier will expand more than the PCB. Figure 1.2 shows a schematic of a row of interconnects subjected to thermal loading. Figure 1.2 (a) depicts the shape of interconnects at some reference temperature, T. Figure 1.2 (b) depicts the deformed shape of interconnects at some maximum temperature, T_1. Finally, Figure 1.2 (c) shows the deformed shape of the interconnects at some minimum temperature, T_0. As the distance between the interconnect and neutral point of package increases, the shearing stresses at solder joints also increases in magnitude. Hence this shear stress induces Mode II loading which leads to interconnect fatigue failure in the BGA package. Most of these fatigue failures occur at the corners of the package. As shown in Figure 1.3 these fatigue cracks typically form in the solder material close to solder/pad interfaces.

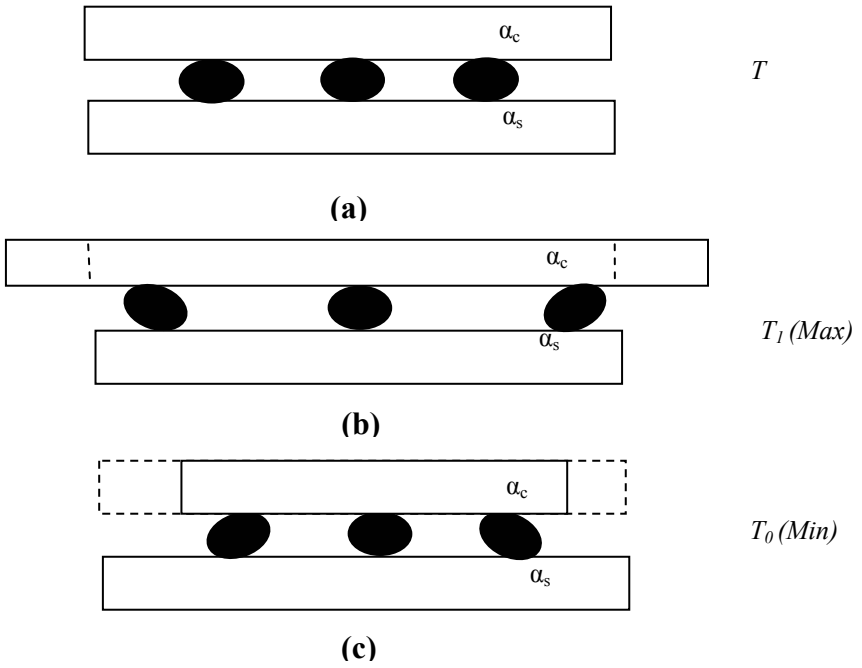

Figure 1.2 Schematic of row of interconnects subjected to thermal cycling. (a)The shape of interconnects at some reference temperature, *T*. (b) The deformed shape of interconnects at some maximum temperature, T_1. (c) The deformed shape of interconnects at some minimum temperature, T_0.

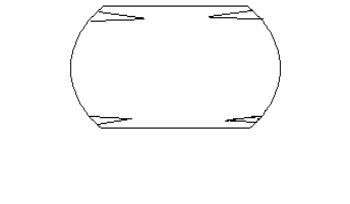

Figure 1.3 Schematic showing the crack prone areas in the solder.

While many researchers have investigated this Mode II shearing of solder joints, Mode I loading can be introduced by several factors including warpage, a mechanical constraint, or the presence of underfill. Underfills are typically polymeric adhesives with a glass transition temperature in the neighborhood of 125°C and act elastically at room temperature. Underfill is usually dispensed as a drop of liquid to fill the volume between the solder interconnects. The liquid is allowed to wick between the package and PCB which subsequently cures to a solid.

Most commonly used underfills exhibit unconstrained shrinkage of up to 3% or more in volume. This contraction that tends to pull the package closer to PCB, is limited by the presence of solder interconnects thus inducing compression in the interconnects in axial direction. The primary purpose of an underfill is to reduce the solder strain by mechanically coupling the die and the PCB. Hence the presence of underfill acts to prolong the fatigue life of BGA package.

While several researchers have focused on the development of the compressive hydrostatic stresses in the solder as a result of underfill curing, the primary goal of this work deals with investigating the significance of axial (Mode I) cyclic stresses that may be induced in the presence of thermal cycling. Hence a finite element model of the solder in the underfill material is developed using Ansys. The following chapter presents the current fatigue life models and discusses thermal cycling effects in a BGA package. Chapter 3 deals with the detailed development of finite element model of the geometry used to study the influence of underfill material properties on the axial stresses that are induced in the solder connections. Chapter 4 discusses the influence of underfill properties on axial stresses as well as the significance of these stresses. This chapter also discusses how these results may be used in the development of a sophisticated fatigue life model based on a fracture mechanics approach. Chapter 5 summarizes the conclusions and recommendations for future work which would refine our understanding of how an underfill effects the fatigue life of a BGA package.

2. Literature Review

As mentioned in the introduction, thermal cycling tests are generally used in electronic packaging industry to predict the reliability and thermal fatigue failure in solder joints [Kaga et.al, (1999)]. When an electronic package is subjected to thermal cycling, the solder interconnects experience shear due to thermal expansion mismatch loading and hence causes the crack to initiate and propagate in the solder. This chapter discusses the thermal cycling effects which induces Mode II shear, the effect of underfill which induces Mode I compressive force to inhibit the crack growth, as well as a literature review of various fatigue life models.

2.1 Basic Fatigue Life Approaches

For over a century, researchers have proposed different life prediction techniques for determining fatigue life. Fatigue life models can generally fall into three different approaches: (a) the strain-based approach, (b) the energy-based approach, and (c) the fracture-based approach.

Strain approach

The strain based approach to fatigue life prediction of a solder joint correlates the plastic strain to the life of the joint. Coffin and Manson developed an equation for low cycle fatigue which results due to irreversibility in plastic deformation during cycling. Considering the mechanical hysteresis, after straining and reversing the load to pull back to the initial condition, all of the discontinuities which lead to plastic deformation do not regain to their initial position. This irreversibility leads to fatigue crack formation which ultimately propagates to failure of the

joint. The fatigue life of the most of the solders which experience shear strain can be predicted using this strain based approach.

The simple power law equation proposed by Coffin-Manson which relates the plastic strain, $\Delta\gamma_{p,}$ to the fatigue life is given by

$$(N_f)^{\alpha}\ \Delta\gamma_p = \Theta \quad (1)$$

where N_f is the fatigue life, α is the fatigue ductility exponent and Θ is the fatigue ductility coefficient. The slope of log-log curve between number of cycles required to failure and plastic strain determines the fatigue ductility exponent.

Energy approach

The energy-based approach for fatigue life prediction relates the mechanical hysteresis energy, W, with the number of cycles to failure. Morrow (1965) was one of the first modern fatigue researchers to show that fatigue life could be correlated with the mechanical energy of the hysterisis loop. This method recognizes that stress is required to move the dislocations required for irreversible local plastic deformation. Nearly all of the energy which is imparted goes in to heat whereas a fraction of this energy is assumed to damage the material which results in failure of the joint. Hence energy approach can be expressed as

$$N_f^m\ W = \Theta_E \quad (2)$$

Where N_f is the fatigue life, W is the hysterisis energy and Θ_E and m are constants.

Fracture mechanics approach

The fracture mechanics approach mainly deals with the crack growth rate to determine the fatigue life of the solder joint. Fatigue can be defined as a process of crack initiation and crack propagation. This crack propagation approach correlates crack growth rate to change in stress intensity factor due to cyclic loading. As figure 2.1 illustrates, there are three types of loading

that a crack can experience: (a) Mode I loading, (b) Mode II loading, and (c) Mode III loading. A cracked body can be loaded in any of these modes or a combination of two or three modes.

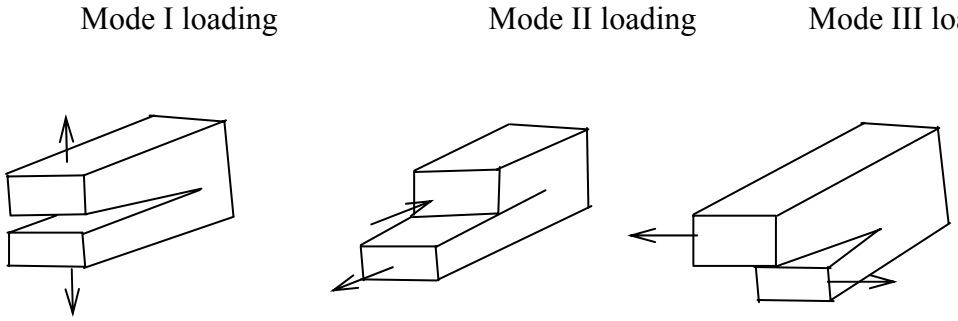

Figure 2.1 The three types of loading that can be experienced by a crack.

A Mode I loading is an opening or a tensile mode of loading where principal load is applied normal to the crack plane where the crack faces are pulled apart. Mode II refers to in-plane shear loading and tends to slide one crack face with respect to the other. Mode III corresponds to out-of-plane or tearing shear where the crack surfaces move parallel to the leading edge of the crack and relative to each other. Paris and Erdogan (1963) were the first to discover the power law relationship for fatigue crack growth and hence the equation is popularly known as Paris law which is described as

$$\frac{da}{dN} = C\Delta K^{m} \tag{3}$$

where $\frac{da}{dN}$ is the crack growth per cycle and ΔK is the maximum and minimum stress intensity developed per cycle and C and m are material constants that are determined experimentally. Hence the number of cycles to failure can be obtained by integrating the above equation. Here the crack tip conditions are uniquely characterized by a single loading parameter such as stress intensity factor and this concept is termed as similitude in fracture mechanics.

2.2 Fatigue Life of Solder Connections

The primary concern for interconnect failure is from the resulting shear caused due to difference in thermal expansion between the chip and PWB in the presence of cyclic temperature variations. As a result the induced shear is assumed to be displacement-controlled and thus the magnitude depends upon the distance of particular interconnect from the center, or neutral point, of the array denoted as *L* in figure 1.2. As the temperature is increased from *T* to T_1, assuming $\alpha_p > \alpha_c$ the resulting thermal or shearing displacement, Δ, of the bottom of the joint with respect to the top is

$$\Delta = (\alpha_p - \alpha_c)(T_1 - T)\frac{L}{2} \tag{4}$$

where α_p and α_c are the coefficient of thermal expansion of the PCB and the chip carrier and (*L/2*) is the distance of interconnect from the neutral point of the package (The neutral point is the point where there is no relative sliding displacement between the surfaces).The nominal shear stress τ can be expressed as

$$\tau = \frac{\Delta}{h} G = \frac{\Delta}{h} \frac{E}{2(1+\upsilon)} \tag{5}$$

where *h* is the height of the interconnect and *G* is the shear modulus. The temperature change is the most common cause of solder joint cracking in electronic packages which leads to strains in solder joints due to thermal expansion mismatch between various materials resulting in fatigue failure [Nemeth et.al, (2000)]. Due to this thermal mismatch the shear strain associated with the interconnects can be expressed as:

$$\gamma = \frac{\Delta \alpha \Delta T L}{h} \tag{6}$$

where $\Delta\alpha$ is the difference between the coefficient of thermal expansion between the PWB and the chip and ΔT is the change in temperature that causes resulting strain.

Vaynman and McKeown (1991) proposed a strain energy partitioning approach for modeling the fatigue behavior and assumed that fatigue damage caused during each cycle is proportional to plastic hysterisis energy per cycle which is replaced by damage function consisting of both stress and strain rate component to predict the fatigue life of solder. In research performed by Solomon and Tolksdorf (1995), they concluded that the plastic strain governs the fatigue life.

In order to compensate for the effect of these stresses and strains during thermal fatigue, an underfill is introduced into the gaps between the solder interconnects. Sitaraman et al. (2001) tested the effect of underfill on SBGA (super ball grid array) packages. Three types of underfills were examined in this study. They observed that the properties of underfill play a vital role in reliability of BGA packages; e.g., a low coefficient of thermal expansion and high modulus underfill significantly reduces solder strain. Hung et al. (2000) underfilled the solder joints with 15 packages of flex type BGA and tested for more than 8 months in a test chamber and found no defects in the packages. They noticed no failure in these solder joints even after 5800 cycles. Liji et al. (2002) investigated failure mechanisms and cycles to failure for two groups of PBGA (Plastic Ball Grid Array) samples both with and without underfill. It was observed that the sample with no underfill failed after 500 cycles whereas the sample with underfill survived without a crack even after 2700 cycles. This clearly shows that underfill can very well protect the solder ball and can act to increase the life of BGA package. FEM simulations were also performed to calculate the maximum stress in the solder balls with and without underfill. The maximum stress induced in the solder with underfill was 60.3MPa while

the maximum stress without underfill was 78.4MPa. While improving the life of a solder joint using underfill it was suggested that careful attention is needed about other modes of failure like warpage etc.

Burnette et al. (2000) conducted an experiment on underfilling ceramic BGA packages using four types of epoxies with different coefficients of thermal expansion and moduli of elasticity. Their experimental results proved that the board level reliability for Ceramic Ball Grid Array packages was greatly increased by using underfill epoxy. In addition, the coefficient of thermal expansion of underfill was one of the important parameters that contributes to the reliability of packages.

2.3 Fracture Model for Solder Connections

Fracture mechanics approaches have become a beneficial tool in characterizing crack growth caused by fatigue. The most common equation used in determining the fatigue life of a cracked component or structure subjected to a single Mode of loading is the Paris law. Other researchers have modified this equation to include other parameters. For instance, Forman suggested the following relationship:

$$\frac{da}{dN} = \frac{C\Delta \mathrm{K}^{m}}{\left(1-\frac{K_{\min}}{K_{\max}}\right)K_{crit} - \Delta \mathrm{K}} = \frac{C\Delta \mathrm{K}^{m-1}}{\left(1-\frac{K_{\max}}{K_{crit}}\right)} \tag{7}$$

where K_{max} is the maximum stress intensity factor, K_{min} is the minimum stress intensity factor, and $\Delta K = K_{max} - K_{min}$. This modification serves to include the fracture toughness of the material, $K_{crit,}$ as an important parameter in determining the fatigue life. Pao (1992) developed a fatigue life prediction approach based on fracture mechanics approach (Knecht Fox formulation) in which fatigue crack growth is controlled by J-integral and C^{*}. This type of formulation is of

importance when plasticity is present. Elber (1970) proposed a fatigue crack growth equation which is a modified form of Paris Erdogan equation and is given as

$$\frac{da}{dN} = C\Delta K_{eff}^{m} \tag{8}$$

where $\Delta K_{eff} \equiv K_{max}$-$K_{op}$ in which K_{max} is the maximum stress intensity factor, K_{op} is the stress intensity at which crack opens, $\frac{da}{dN}$ is the fatigue crack growth per cycle, and C and m are material constants determined experimentally.

When using the above equations only one Mode of loading can be considered. For example, when dealing with the thermal fatigue of solder connections, typically a Mode II cyclic loading is considered when predicting the fatigue life of the connections. As one can imagine, the addition of a tensile loading should act to grow the crack more quickly while the addition of a compressive loading should act to close the crack and therefore, inhibit it from growing as quickly. Refer to figure 2.2. Larson and Verges (2003) developed a fracture-based fatigue life model based on this concept assuming that the Mode I component is constant.

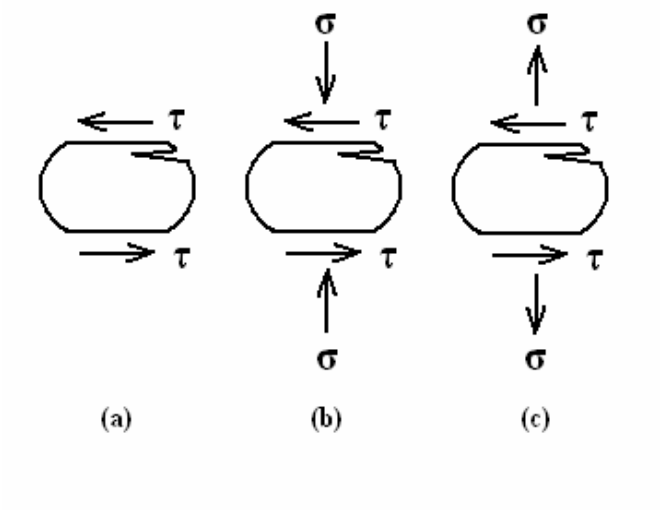

Figure 2.2 Schematic depicting stresses on an edge crack. (a) Mode II shear stress. (b) Shear stress with an additional compressive Mode I stress. (c) Shear stress with an additional tensile Mode I stress.

They plotted the relative life prediction equations which show that an axial tension along with shearing decreases the fatigue life whereas the axial compression along with shearing increases the fatigue life of interconnects. Hence the equation for relative increase in the fatigue life due to axial compression was given as

$$\frac{N}{N} = \left(\frac{\pi\gamma}{\pi\gamma + \mu(\frac{f}{Gr2})} \right) \tag{9}$$

where $N^{(c)}$ is the fatigue life when interconnect is subjected to axial compression, $N^{(o)}$ is the fatigue life in absence of an axial load, f is the axial force, r is the radius of the interconnect, γ is the shear strain, and μ is the friction coefficient.

In order to enhance the reliability of solder joints, a constant Mode I compressive loading can be introduced by several factors including a mechanical constraint or the presence of underfill. Most commonly used underfills exhibit unconstrained cure shrinkages of up to 3% or more in volume. This contraction that tends to pull the package closer to the printed wiring board, is limited by the presence of solder interconnects thus inducing compression in the interconnects in the axial direction. Initially, the contraction of the underfill will also cause the solder to undergo tension in the radial direction. Larson et al. (2004) modeled underfill curing in a BGA package. They concluded that after the solder is allowed to creep, the final steady state stresses are in hydrostatic compression.

Larson et al. (2004) also developed an equation using nonlinear finite element analysis to predict the steady state stresses caused by contraction of the underfill upon curing using ABAQUS. They tested for various ranges of underfill properties (E_u=0.5 to 8.0GPa, v_u=0.2 to 0.4 and $\%sh_u$ = 0.2% to 1.0%) and developed the following expression

$$\sigma_s = (A\,(E_u/\sigma_y)+B)*\%sh_u*E_u/(1-\nu_u) \quad (10)$$

for estimating the influence of underfill parameters such as $\%sh_u$, E_u, and ν_u on steady state compressive stresses. In this equation σy is the yield stress of the solder and is taken to be 33MPa, A= 2.94x10^{-6}, B= -2.85x10^{-3} and $\%sh_u$ is the linear percentage shrinkage of underfill material.

While there presently is not a fracture-based model aimed at determining the fatigue life of packages subjected to mixed-mode cyclic loading, experimental efforts in this area are also lacking. Yao et al. (1996) developed an experimental technique known as flexural peel technique to study the crack growth in solder joints under mixed mode loading conditions. This experiment consists of a three layered arrangement in which the Sn-Pb specimen is sandwiched between two copper layers of different lengths. This specimen is placed on to a test apparatus and loaded in flexural peel mode. One end of the specimen was fixed to a bending load cell and the other end was peeled using pull rod connected to a mechanical actuator to induce mixed-mode loading conditions.

3. Finite Element Model

A finite element model is developed to predict the influence of an underfill on the Mode I loading of an interconnect in a BGA package in the presence of thermal cycling using Ansys 7.1. The finite element geometry of the solder interconnect implemented here is the same as considered by Larson et al. (2004). The primary assumptions are that the solder interconnections are a part of infinite array and that the geometry of the connections has a negligible effect on the normal stresses. This second assumption allows the solder to be modeled as a cylinder. Therefore the geometry considered for the finite element model is a unit cell of two concentric cylinders. The outer cylinder represents the underfill and the inner cylinder represents the solder connection as shown in figure 3.1.

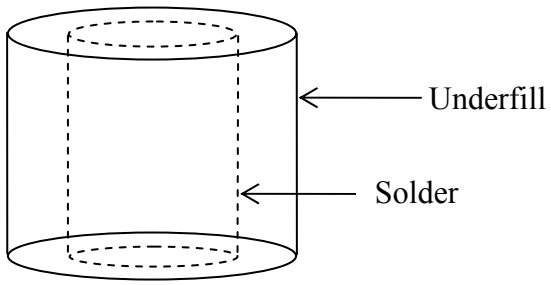

Figure 3.1 A three dimensional view of a unit cell. The inner cylinder is representative of the solder connection while the outer cylinder is representative of the underfill.

The solder modeled in the analysis is a eutectic composition of lead and tin which is commonly used in electronic packages as both mechanical and electrical connections because of its

favorable wetting property. The underfill modeled in the analysis is a polymeric adhesive which can produce a beneficial compression upon shrinkage in BGA interconnects. This finite element analysis is developed using general purpose ANSYS code which is included in *Appendix A*. The analysis methodologies implemented in the ANSYS software code are discussed in detail in each section of this chapter.

3.1 Finite Element Geometry

The actual finite element geometry is an axis-symmetric model of a unit cell cross section as shown in Figure 3.2. The two dimensional finite element model is constructed with 4-noded PLANE 182 axis-symmetric elements. The element selection and descritization are two important assumptions which play a key role in finite element model. The choice of type of element used depends on the number of degrees of freedom needed to which the physical structure can be modeled without any approximation. The dimensions of the geometry are chosen such that the unit cell is representative of commonly used area array packages such as BGA's, chip scale and flip-chip packages; i.e., the height of the interconnect is 0.5mm, the radius of the pad is 0.4mm, and the pitch (the distance between the connections) is 1.27mm. Therefore, for the cross-section shown in Figure 3.2(b) the overall width of the model is 0.635 mm, (half of the pitch). The overall height, which as shown in Figure 3.2(a) is the half-height of the solder connection, is 0.25 mm. These dimensions are noted in figure 3.3.

(Referring to the ANSYS code in *Appendix A*, Lines 1 through 6 in section 3.1 denotes the creation of key points necessary to generate the two rectangular areas. For example in line 1, the *k* represents that a key point is being defined and, the *1* denotes the reference number for the key point. The coordinates *0,0* denote the key point location in the active coordinate system. The rectangular areas are created in lines 7 and 8. Referring to line 7, the *A* represents that an area is

being created by connecting key points. The numbers *1,2,3,4* denote the list of key points defining the area).

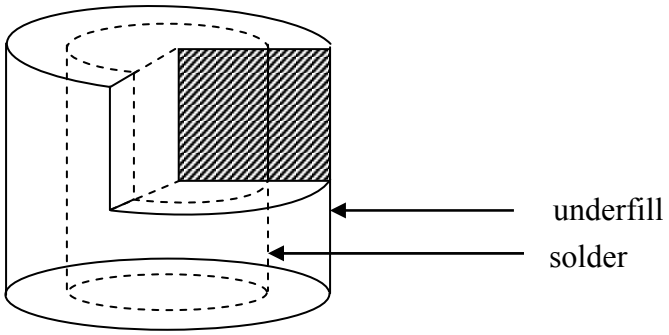

(a)

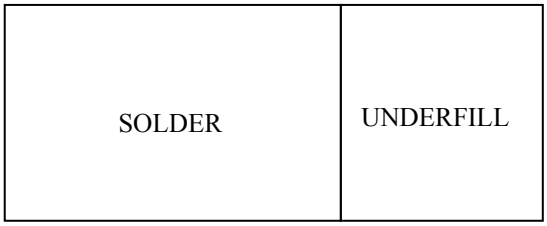

(b)

Figure 3.2 (a) Schematic of three-dimensional view of the unit cell with a highlighted section showing the cross-sectional view of the finite element geometry. **(b)** Schematic of the two dimensional geometry used in the creation of the axisymmetric finite element model.

3.2 Boundary Conditions

The nodes at the solder/underfill interface are not allowed to separate and are glued allowing sharing of interface nodes.(Referring to *Appendix A*, in section 3.1, line 9 denote the gluing of both the rectangular areas in which *AGLUE* generates new areas by gluing existing areas and *ALL* denotes that all the selected areas to be glued.) According to the geometry shown in Figure 3.3, the left most boundary of the unit cell is considered as an axis of symmetry. Hence the movement of these nodes is constrained in the x-direction. (Referring to *Appendix A*, this boundary condition is created in line 18 and 19 in section 3.2, For example, in line 18, *NSEL*

denotes selecting the subset of nodes, *S* denotes selecting a new set of nodes, *LOC* denotes the location, *X* denotes the x-component, *0* denotes the location of the x-component. In line 19, *D* denotes the degrees of freedom constraints at selected nodes, *ALL* denotes applying the constraints for all selected nodes and *UX* denotes the degrees of freedom on x-direction.) Due to the unit cell assumption, the movement of nodes on outer edge of underfill, i.e. the right most boundary, is also constrained in x-direction. (Referring to *Appendix A,* lines 22 and 23 in section 3.2 refers to this boundary condition.) The nodes on the lower boundary are constrained to move in the y-direction because this boundary is physically located at the half-height of the interconnect. (Referring to *Appendix A*, lines 15 through 17 in section 3.2 refers to this boundary condition.) The nodes on the top edge of the unit cell, which represent the solder/pad and underfill/substrate interface, are constrained from movement in the x-direction because physically the solder and underfill adhere to the pad and substrate. (Referring to *Appendix A*, lines 20 and 21 in section 3.2 refers to this boundary condition.) Also, the top edge is constrained to move uniformly in y-direction. Because the substrate and PCB are much stiffer than solder and underfill materials, this restriction forces the top boundary to remain planar. (Referring to *Appendix A*, lines 1 through 14 in section 3.2 contains the methodology for developing constraint equations to implement the above boundary condition. For example in line 1, *CE* defines the constraint equation relating the degrees of freedom, *1* denotes equation reference number, *0* denotes the constant term of the equation, *42* denotes the node number for first term of equation, *UY* denotes the degrees of freedom label for first term of equation, *1* denotes the coefficient for first node term of the equation, *61* denotes the second node number, *UY* denotes the degrees of freedom label for second term of equation, *-1* denotes the coefficient for second node term of the equation.)

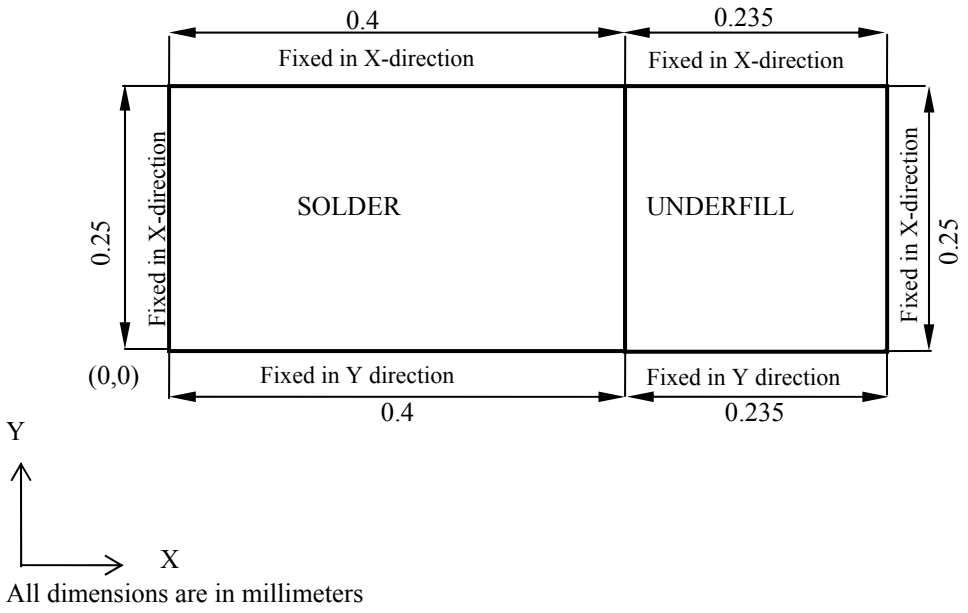

Figure 3.3 Schematic of finite element geometry with the dimensions and boundary conditions.

3.3 Material Constituents

The material properties of solder are taken to be that of a eutectic Sn-Pb solder which is commonly used in most applications. As such, the modulus of the solder material, E_s, was taken to be 32GPa, Poisson's ratio, v_s, was taken to be 0.3, coefficient of thermal expansion, α_s, was taken to be 24.1×10^{-6}/K and the yield stress, σ_y, was taken to be 33MPa. Due to its unique properties, solders are well suitable for many applications and insure their continuous use. The low melting point of eutectic Sn/Pb (183°C) allows the solders joints to be fabricated at lower temperatures. Moreover, these solders are very ductile and Sn/Pb can be super plastic. This ductility allows the solder to have exceptional thermal resistance allowing their use under conditions where other materials fail.

The underfill material properties considered are exemplar of a range of commercially available underfills. As such, the modulus of elasticity of underfill, E_u ranges from 2.0 GPa to 8.0

GPa, Poison's ratio υ, ranges from 0.2 to 0.4 and the coefficient of thermal expansion, α_u ranges from $10x10^{-6}$ / K to $100x10^{-6}$/ K. Hence the Young's moduli of 2.0, 3.5, 5.0, 6.5, and 8.0 GPa were considered. In addition Poisson's ratio of 0.2, 0.3, and 0.4 were considered as well as coefficients of thermal expansion of $10x10^{-6}$/K, $40x10^{-6}$/K, $70x10^{-6}$/K, and $100x10^{-6}$/K. This resulted in 60 combinations of underfill properties tested.

(Referring to *Appendix A*, lines 1 through 9 in section 3.3 contain the material properties for both the solder and underfill material. For example, in line 1, *MP* defines the material property, *EX* denotes the material property label for modulus of elasticity, *1* denotes the material reference number, and *32E9* denotes the modulus of elasticity for the solder material.)

3.4 Thermal Loading

The effect of an underfill on the solder joint fatigue life in aerospace applications is investigated in this research. Usually the board temperature in the space craft in an aerospace environment fluctuates $\pm 20°$ C, about room temperature during one cycle [Bjordahl et.al, (1997)]. Geo Synchronous Earth Orbit (GEO) missions cycle once a day where as Low Earth Orbit (LEO) missions undergo thermal cycling 16 to 24 times a day. Because solder require ample time for creep behavior to become significant at these temperatures, creep is not considered in this analysis.

To model this thermal loading, a static analysis is performed for two different load cases :(a) 25°C to 5°C and (b) 25°C to 45°C. The stress pattern corresponding to the displacement when the temperature varies from 25°C to 5°C (298K to 278K) is the same as the stress pattern corresponding to the displacement when the temperature varies from 25°C to 45°C (298K to 318K) because the modulus of elasticity is taken as constant over the temperature range of 5°C to 45°C. For example, if for one case the resulting normal stresses induced in the solder are in

tension then the resulting normal stresses for other case will be in compression. However, the absolute values of the magnitudes of the stresses are equal. Consequently, for all underfill properties tested it was necessary to only perform the static analysis for a loading of 25°C to 5°C to obtain all of the necessary information regarding the magnitude of the normal stresses.

(Referring to *Appendix A*, Lines 1 through 15 in section 3.4 denotes the methodology of applying thermal loading on unit cell geometry. For example, line 1 defines using nonlinear solution defaults and some enhanced internal solution. Line 2 defines the default time for the load step. Line 3 defines the default time step size to be used for the present load step. Line 4 defines the solution data written to the database. Line 5 defines the solution output written to the database. Line 6 defines the uniform temperature of 298K for the present load step. Line 7 defines solving the load step. Line 8 defines saving all current database information. Line 12 defines the uniform temperature reduction to 278K.)

3.5 Convergence Criterion

The finite element geometry is meshed using PLANE 182 axisymmetric 4-noded elements as shown in Figure 3.4. There are 800 elements with 861 nodes. Each element has degrees of freedom in both the *x*-direction and *y*-direction. The number of elements to be chosen for idealization depends upon the accuracy desired, degrees of freedom, etc. Although the increase in number of elements generally yields an increase in accuracy of the results, there will be certain number of elements beyond which the accuracy cannot be improved by any significant amount. This is termed as convergence of the solution. This convergence is an important factor to be considered in finite element modeling. In this work, convergence of the solution was tested by choosing meshes with 200, 800 and 1600 elements. It was observed that there was no significant improvement in the values of the normal stresses beyond meshing with more than 800

elements. Figure 3.5 gives an example of the normal stresses obtained for three different meshes. For this case the underfill properties were E_u=3.5GPa, ν_u=0.3, and α_u= 100x10^{-6}/K. The thermal loading is applied as the temperature is decreased from 25°C to 5°C. The graph depicts the normal stress values along the top boundary of the solder connection. The difference in the values of the normal stresses between 800

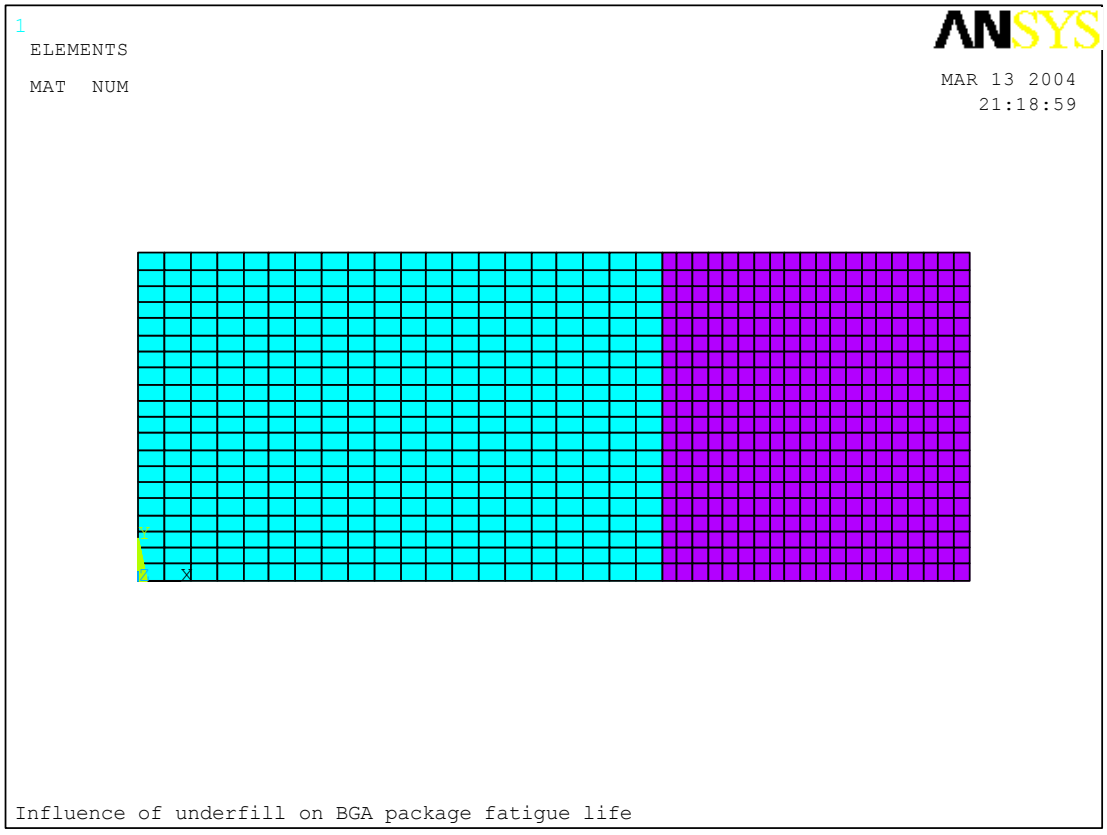

Figure 3.4 Ansys plot showing the mesh of finite element geometry.

elements and 1600 elements was restricted to 0.01 percent. As a result, 800 elements were used in the finite element model.

(Referring to *Appendix A*, lines 1 through 6 in section 3.5 denote the meshing of the solder material and lines 7 through 11 denote the meshing of underfill material in the finite element geometry. For example, a material number is assigned to the subsequently defined

elements in line 1. In line 2, *LESIZE* specifies the divisions of unmeshed lines, *1* denotes the line number to be divided, *20* denote the number of element divisions per line. In line 6 the nodes and elements are created within the generated area 1.)

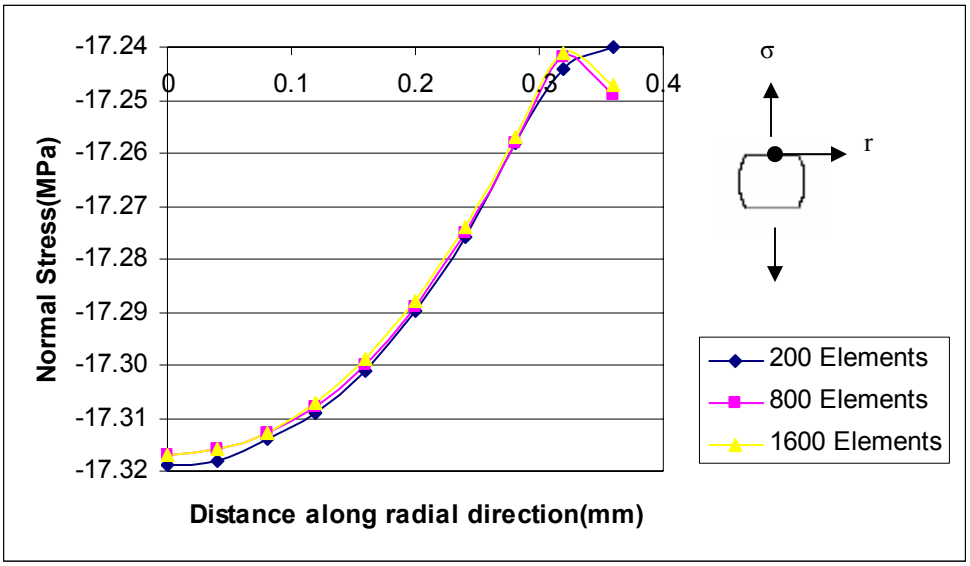

Figure 3.5 Graph depicting the convergence criterion for normal stress values along the top boundary of the solder interconnection. The underfill material properties for this case E_u=3.5GPa, v_u=0.3, and α_u=100X10^{-6}/K. The temperature loading is from 25°C to 5°C.

4. Results

The influence of underfill material properties on the normal stresses in the solder connections was investigated using the finite element model of the unit cell cross section of the BGA package discussed in chapter 3. A thermal loading representative of the temperature range maintained in aerospace applications was applied to obtain the normal cyclic stresses induced at the solder/pad interfaces. In the analysis room temperature is taken to be 25°C. At this temperature the normal stresses are taken to be zero. Figure 4.1 displays the normal stresses along the top boundary of the radius of the solder connection as the temperature is decreased to 5°C. The underfill properties for this case corresponds to E_u=3.5GPa, v_u=0.3, and α_u= 100x10^{-6}/K. Note that the normal stresses across the boundary are similar. For simplicity, in this work the normal stresses for each underfill combination are defined as the normal stress obtained at the node located in the center on the top boundary of the connection. In Figure 4.1 this would be the node located 0mm along the radial direction.

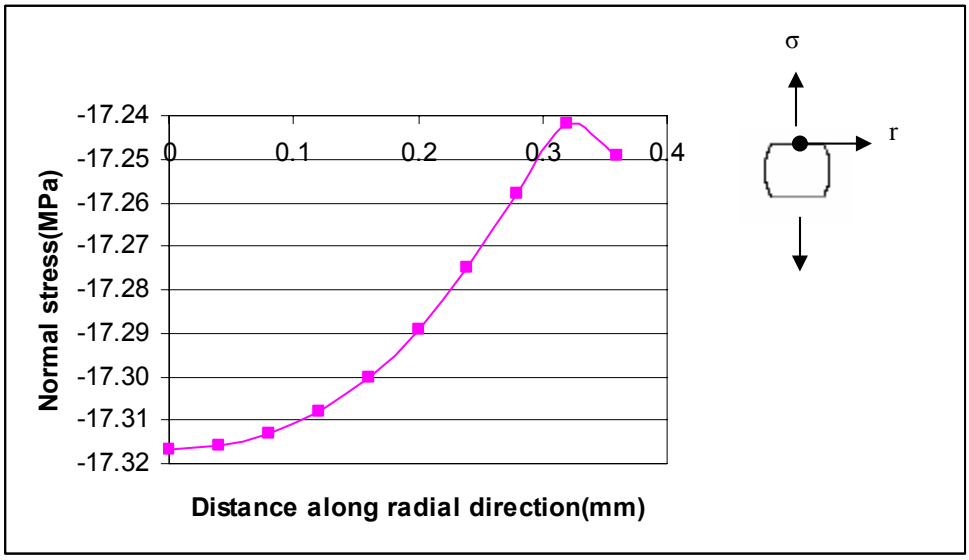

Figure 4.1 Graph depicting normal stress values along the top boundary of the solder interconnection. The underfill properties for this case are E_u=3.5GPa, ν_u=0.3, and α_u= 100x10^{-6}/K. The temperature loading is from 25°C to 5°C.

4.1 Influence of Underfill Parameters

Figure 4.2 displays the magnitude of normal stresses when the temperature is decreased from 25°C to 5°C for Young's moduli of 2.0GPa, 3.5GPa, 5.0GPa, 6.5GPa, and 8.0GPa. Note in figure 4.2(a) that in some cases the normal stress is in tension and in some cases normal stress is in compression. For example when ν_u=0.3, the normal stress is in tension for α_u=10x10^{-6}/K and is in compression for α_u=40x10^{-6}/K, 70x10^{-6}/K, and 100x10^{-6}/K when the temperature is 5°C. Figure 4.3 displays how these normal stresses would fluctuate over one temperature cycle (assuming the cycle is sinusoidal).

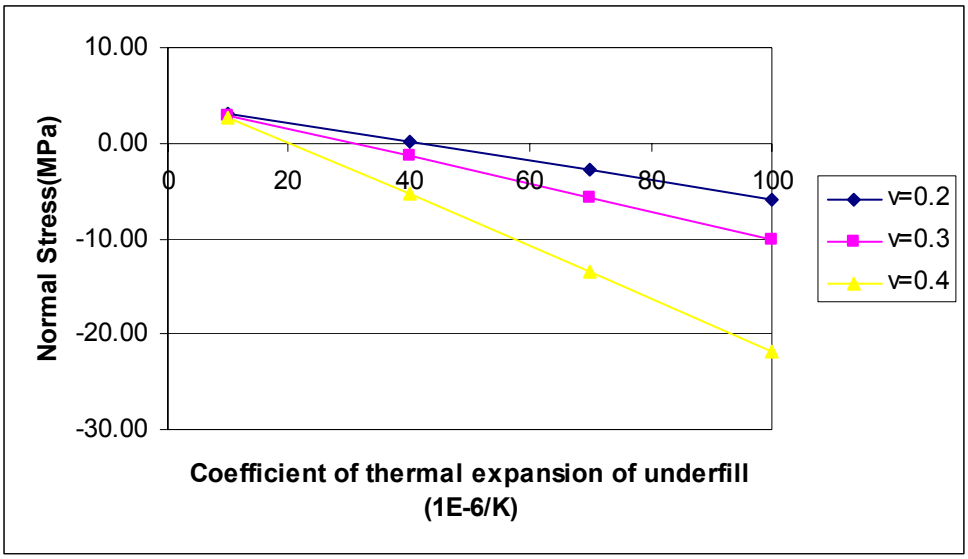

(a)E_u=2.0GPa

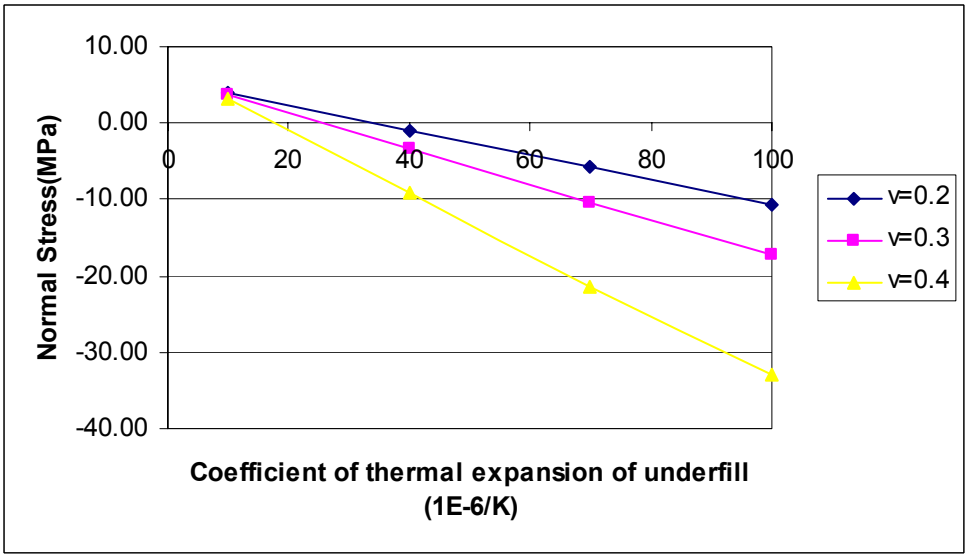

(b) E_u=3.5GPa

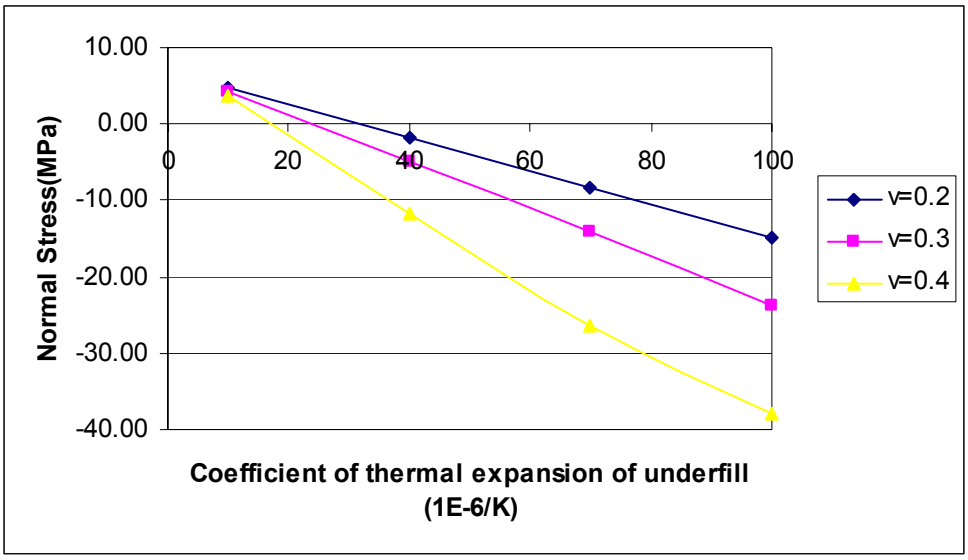

(c) E_u=5.0GPa

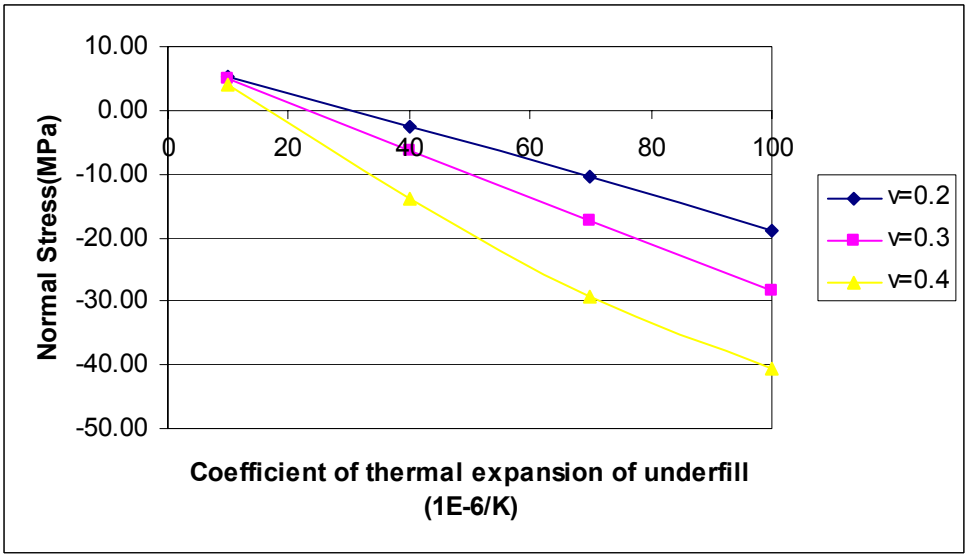

(d) E_u=6.5GPa

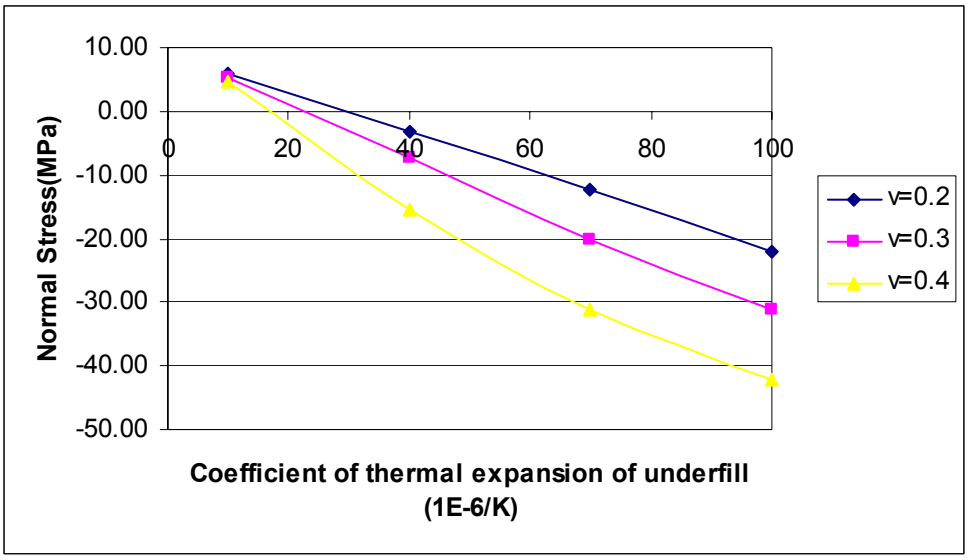

(e) E_u=8.0GPa

Figure 4.2 Graphs depicting the normal stresses at the node located at the middle of the top of the solder interconnect.

Figure 4.2(a) displays the magnitude of normal stresses at 5°C for a Young's modulus of 2.0GPa. As shown in the graph, the normal stresses are becoming greater in absolute magnitude with an increase in the coefficient of thermal expansion of the underfill material. Also, the absolute magnitude of normal stresses increases with increase in Poisson's ratio of underfill material. For the Young's modulus of 2.0 GPa, the coefficient of thermal expansion plays a stronger role in influencing the resulting normal stresses than does the Poisson's ratio.

Figure 4.2(b) depicts the magnitude of normal stresses at 5°C for a Young's modulus of 3.5 GPa. Similar to what is displayed in Figure 4.2 (a), as the coefficient of thermal expansion and Poisson's ratio of the underfill material increases, the stresses become greater in absolute magnitude. Again, the coefficient of thermal expansion plays a stronger role in influencing the resulting normal stresses than does the Poisson's ratio. However, it is evident when comparing the two graphs that as the stiffness of the underfill material increases, v_u and α_u have more of an influence on the resulting normal stresses. For example, when E_u = 2.0 GPa and v_u=0.4, the

normal stresses range from 2.64MPa to 21.8MPa as α_u is increased. When E_u = 3.5 GPa and v_u=0.4, the normal stresses range from 3.11MPa to 32.96MPa. Similarly, when E_u = 2.0 GPa and α_u =100x10^{-6}/ K, the normal stresses range from 5.84MPa to 21.8MPa as v_u is increased. When E_u = 3.5 GPa and α_u =100x10^{-6}/ K, the normal stresses range from 10.7MPa to 32.96MPa.

Note from Figures 4.2(c), (d), and (e) that as the stiffness of the underfill material is increased, the coefficient of thermal expansion continues to display an increasing influence on the resulting normal stresses. However as seen when comparing the normal stresses in Figures 4.1(d) and (e), this increase in influence on the normal stresses is becoming minimized. It is also evident when comparing the figures that for a constant α_u and v_u, an increase in stiffness results in more compressive normal stresses. In addition, as v_u is decreased, the stiffness plays a stronger role in influencing the magnitude of the normal stresses.

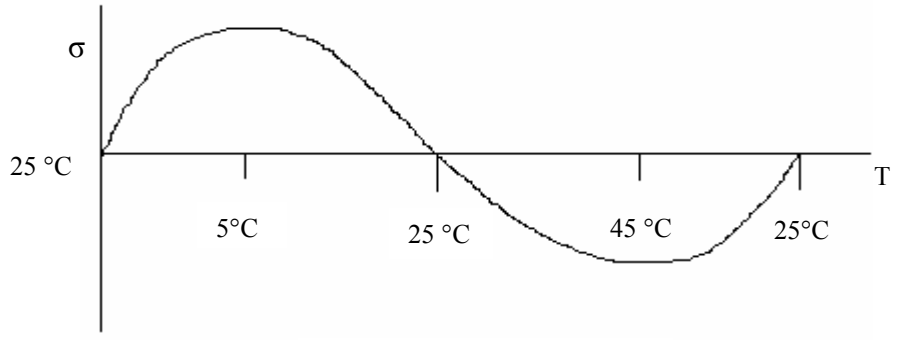

(a) α_u=10x10^{-6}/K

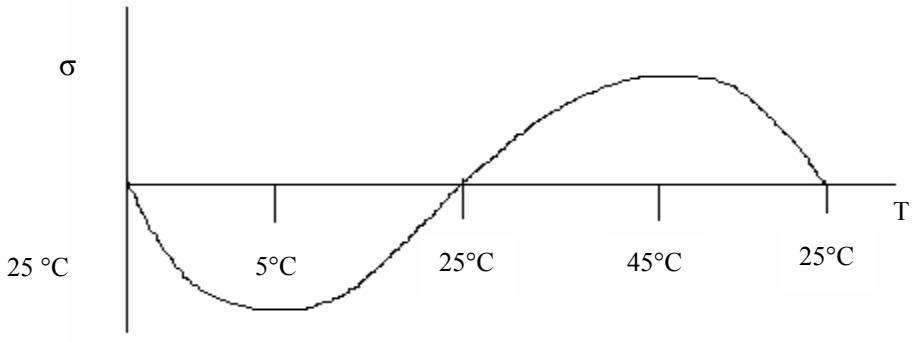

(b) α_u=40x10^{-6}/K

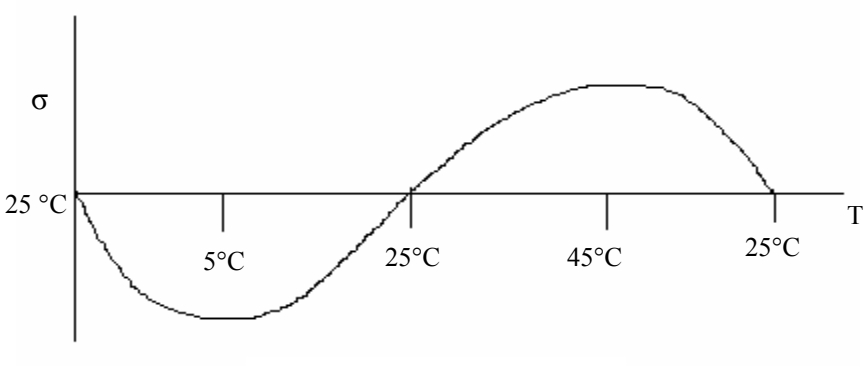

(c) α_u=70x10^{-6}/K

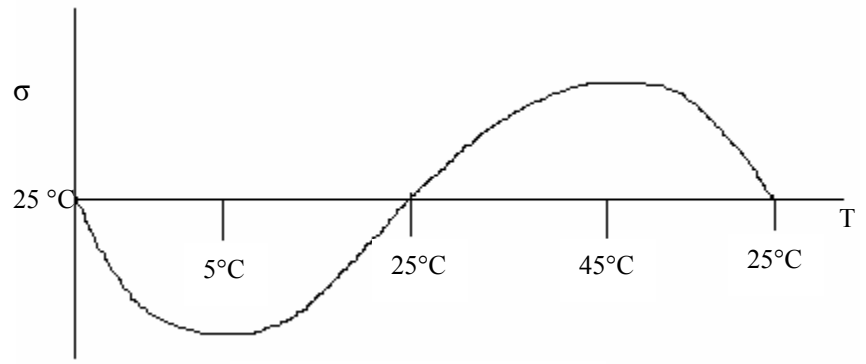

(d) α_u=100x10^{-6}/K

Figure 4.3 Schematic of the fluctuation of normal stresses over a temperature cycle for the case of E_u=2.0GPa and ν_u=0.3 assuming temperature profile is sinusoidal.

In general, as the temperature is decreased, the absolute magnitude of the stresses are increasing with an increase in α_u, E_u, and ν_u. Therefore, the most compressive as well as the most tensile stress for the underfill combination tested is shown in Figure 4.1(e) for the case where E_u=8.0GPa, ν_u=0.4, and α_u=100x10^{-6}/K.

4.2 Significance of Mode I Cyclic Stresses

It was stated in the introduction that much research has centered around predicting the fatigue life of interconnects based on the Mode II shearing induced upon thermal cycling. It was also stated that research has shown that underfill has been used to provide beneficial residual

compression in these connections. Larson et al. (2004) developed an equation using nonlinear finite element analysis to predict the steady state stresses caused by contraction of the underfill upon curing using ABAQUS. As mentioned in chapter 2, they tested for various ranges of underfill properties (E_u=0.5 to 8.0GPa, v_u=0.2 to 0.4, and $\%sh_u$ = 0.2% to 1.0%) and concluded that these resulting steady state stresses were in residual compression.

In the present work equation (10) is used to determine if the Mode I cyclic stresses obtained in the previous section are negligible or significant when compared to the residual stresses induced during curing. The Mode I cyclic stresses are added to the steady state stresses according to the schematic 4.4.

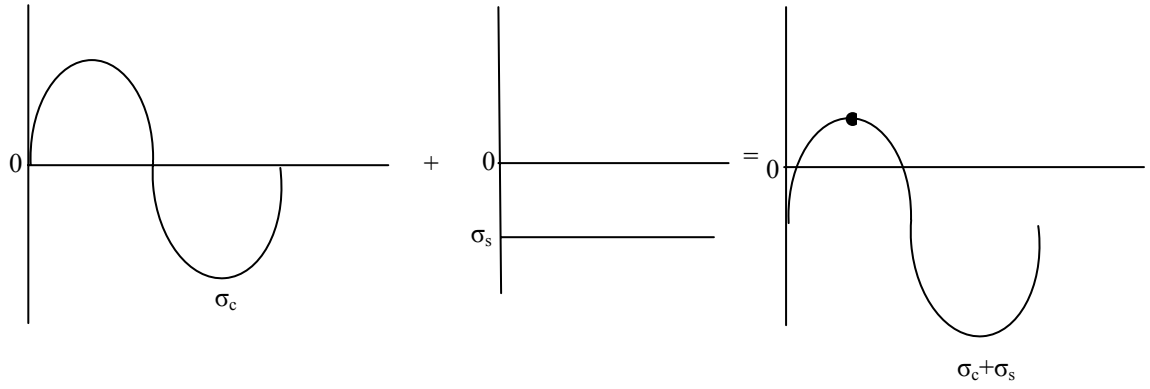

Figure 4.4 Schematic showing the addition of Mode I cyclic stresses to steady state stresses.

Appendix B contains a list of the Mode I cyclic stress obtained from the finite element results, the residual steady state stresses obtained from equation (10), as well as the most tensile stress induced from the combination of the constant residual stress and the cyclic stress for every combination of underfill parameters tested. As seen in *Appendix B*, the resulting cyclic stresses, σ_c, are on the same order of magnitude as the residual stresses, σ_s. The main conclusion from this work is that these Mode I cyclic stresses are not negligible and need to be considered in the development of a fatigue life model of solder interconnects in BGA packages.

Figure 4.5 displays the plots of the most tensile stresses induced in the solder during one thermal cycle. These stresses correspond to the point highlighted on the schematic in the Figure 4.4. For simplicity, it is assumed in Figure 4.5 that the linear shrinkage upon curing is 0.6% of the underfill material.

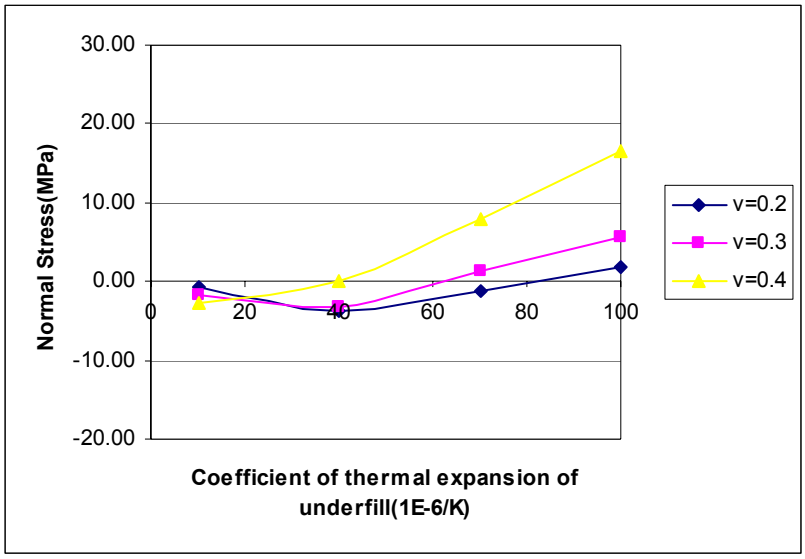

(a) E_u=2.0GPa

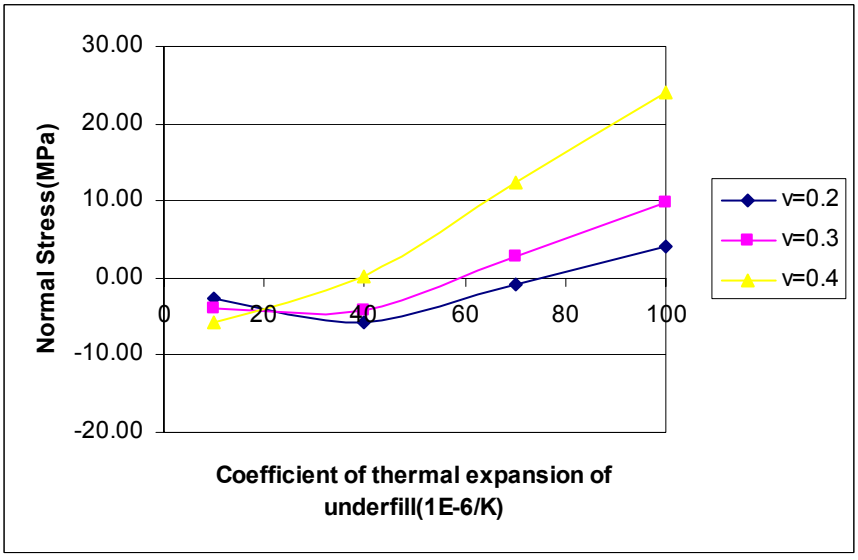

(b) E_u=3.5GPa

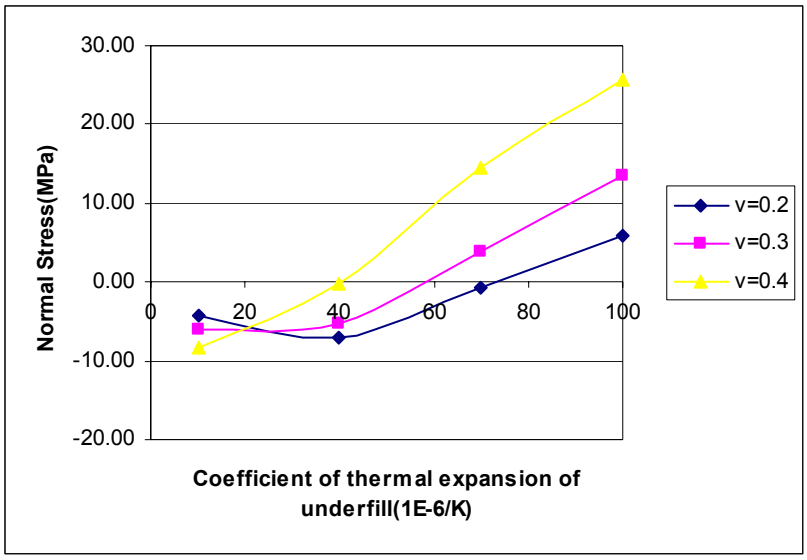

(c) E_u=5.0GPa

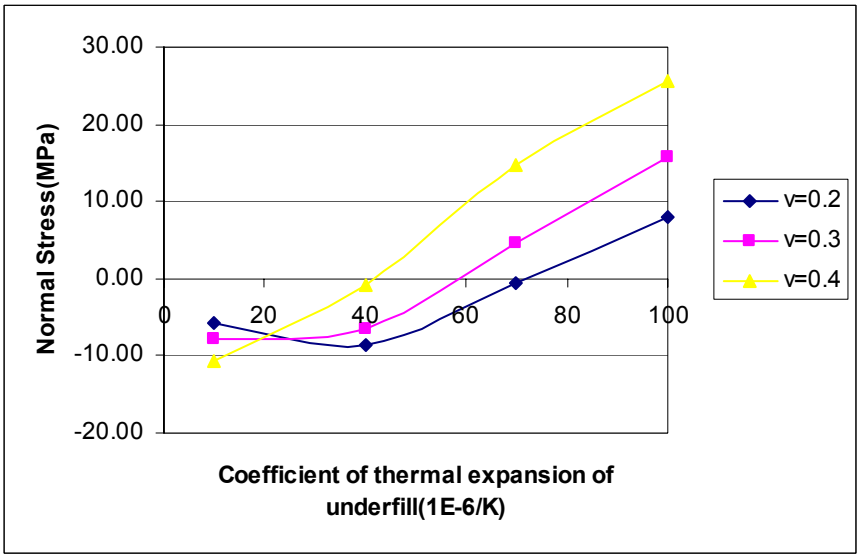

(d) E_u=6.5GPa

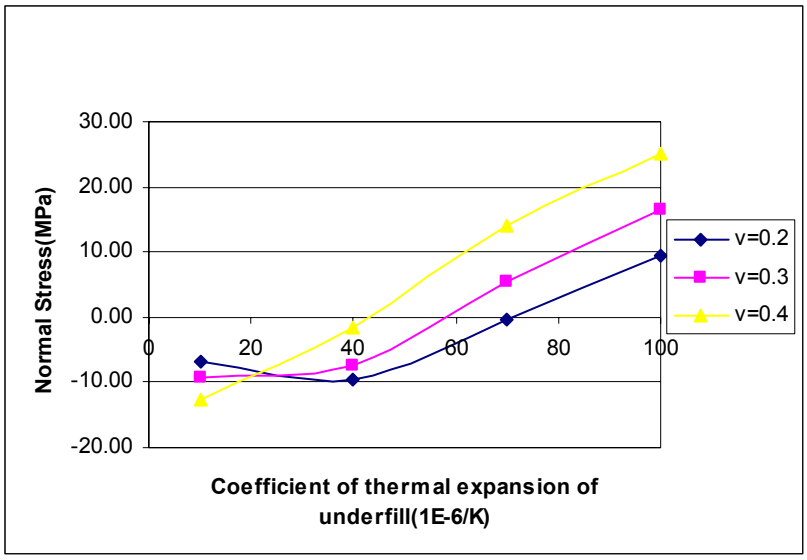

(e) E_u=8.0GPa

Figure 4.5 Graphs depicting the most tensile stresses induced in the solder during one thermal cycle when temperature is 5°C and *%sh* of underfill material is 0.6%.

As depicted in the graph, for a α_u = 10x10^{-6}/K, the stresses are becoming more compressive with stiffer underfill. Also at α_u = 40x10^{-6}/K as the underfill becomes stiffer, the stresses are becoming compressive in nature. For α_u = 70x10^{-6}/K and 100x10^{-6}/K the stresses are becoming more tensile in nature as the stiffness is increased. Also for α_u = 10x10^{-6}/K as the Poisson's ratio increases the stresses are more compressive in nature. For α_u = 40x10^{-6}/K, 70x10^{-6}/K and 100x10^{-6}/K the stresses are becoming more tensile with an increase in Poisson's ratio of the underfill material.

It is interesting to note when observing figure 4.5 the strong dependence on the coefficient of thermal expansion. Note for all material combinations possessing a coefficient of thermal expansion, α_u, greater than around 70x10^{-6}/K, the solder will experience a tensile loading during thermal cycling. Recall, from chapter 2 that this type of loading acts to propagate the crack rather than inhibit its growth.

Referring to *Appendix B*, for $\alpha_u = 10\text{x}10^{-6}$/K as the *%sh* value increases the stresses are becoming more compressive. Also for $\alpha_u = 40\text{x}10^{-6}$/K as the *%sh* value increases the stresses become compressive in nature. Finally, for $\alpha_u = 70\text{x}10^{-6}$/K and $100\text{x}10^{-6}$/K as the *%sh* value increases the stresses are less tensile in nature.

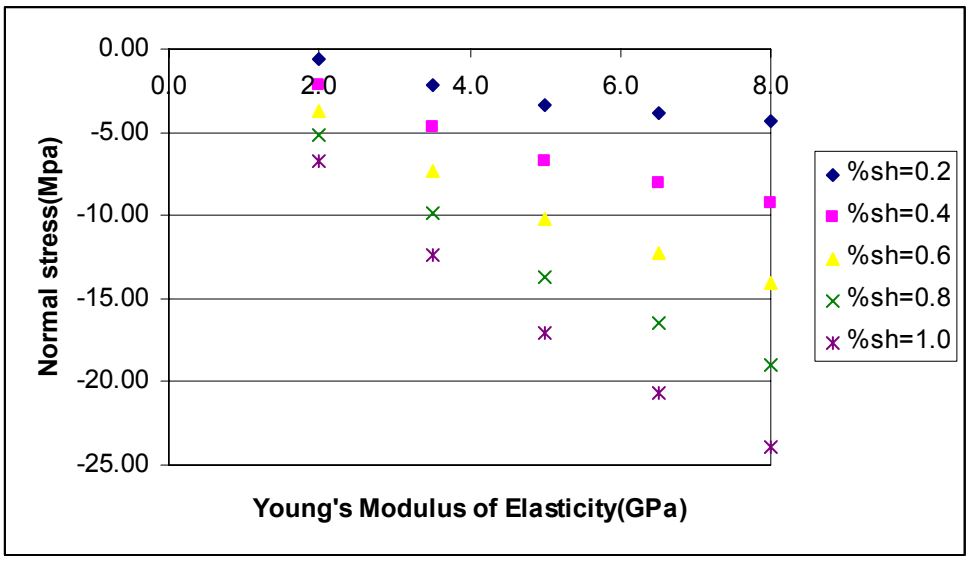

Figure 4.6 Plot depicting the normal stresses for the case when $v_u = v_s$ and $\alpha_u = \alpha_s$.

While underfill materials in use today have stiffness well below that of solder, typical underfills can possess similar Poisson's ratio and coefficients of thermal expansion. Assuming the coefficient of thermal expansion and Poisson's ratio of the underfill are the same as that of the solder material, Figure 4.6 displays the influence of Young's modulus on the normal stresses in the connections. This plot displays the most tensile stresses obtained during one cycle when adding the cyclic stresses to the steady state stresses obtained from equation (10). The plot demonstrates that as the underfill becomes stiffer the stresses are becoming more compressive in nature. Also, as the linear shrinkage of the underfill material increases the absolute magnitude of normal stresses also increases. It can be deduced from this plot that as long as $v_u = v_s$ and $\alpha_u = \alpha_s$, the normal stresses induced in the interconnect during the course of one thermal cycle will always be compressive for this range of Young's moduli and linear shrinkages.

The following are several underfill materials which are commonly used in BGA packages: FP4531 with E_u=7.6GPa, ν_u=0.33, and α_u=28x10^{-6}/K; FP4530 with E_u=5.6GPa, ν_u=0.33, and α_u=43x10^{-6}/K; and 3510 with E_u=2.8GPa, ν_u=0.33, and α_u=70x10^{-6}/K. These material properties are obtained from technical support at Loctite. The Mode I steady state stresses obtained using equation (10) are -12.1 MPa, -12.6 MPa and -9.78 MPa respectively. The most tensile stresses obtained from finite element analysis for these cases are 3.25 MPa, 8.13 MPa, and 10.2 MPa, respectively. The most tensile stresses obtained from finite element analysis were added to the steady state stresses obtained from equation (10). The results are depicted in Figure 4.7.

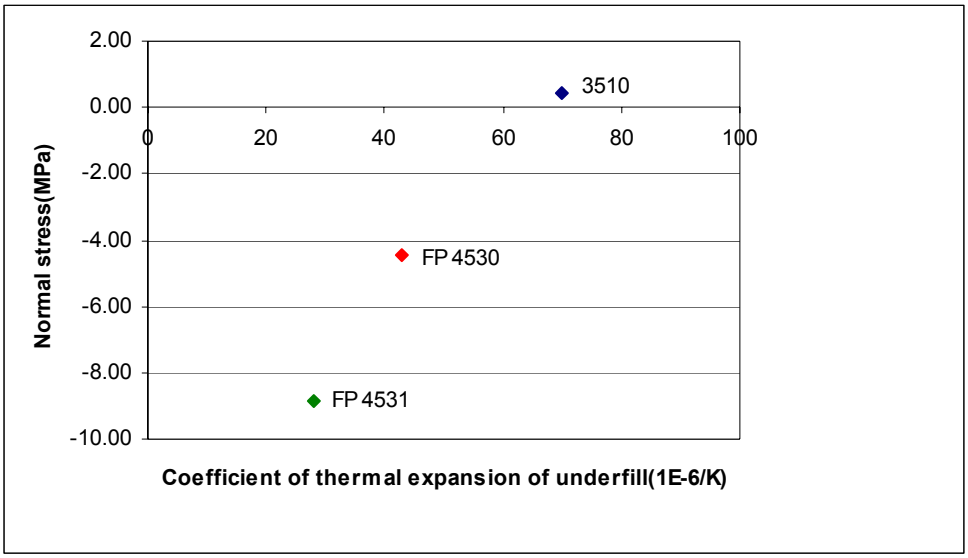

Figure 4.7 Graph depicting the normal stress values for real underfill material properties.

Figure 4.8 displays a schematic of the Mode I cyclic stresses induced in the solder connections during a thermal cycle for the three different underfills. Although the solder in packages containing FP4531 and FP4530 underfills have similar residual stresses, observe that the Mode I stresses in the solder in packages containing the FP4530 underfill fluctuate more than twice as much. In addition, these results show that for a BGA package with 3510 underfill the solder interconnects will experience a tensile loading during the thermal cycle.

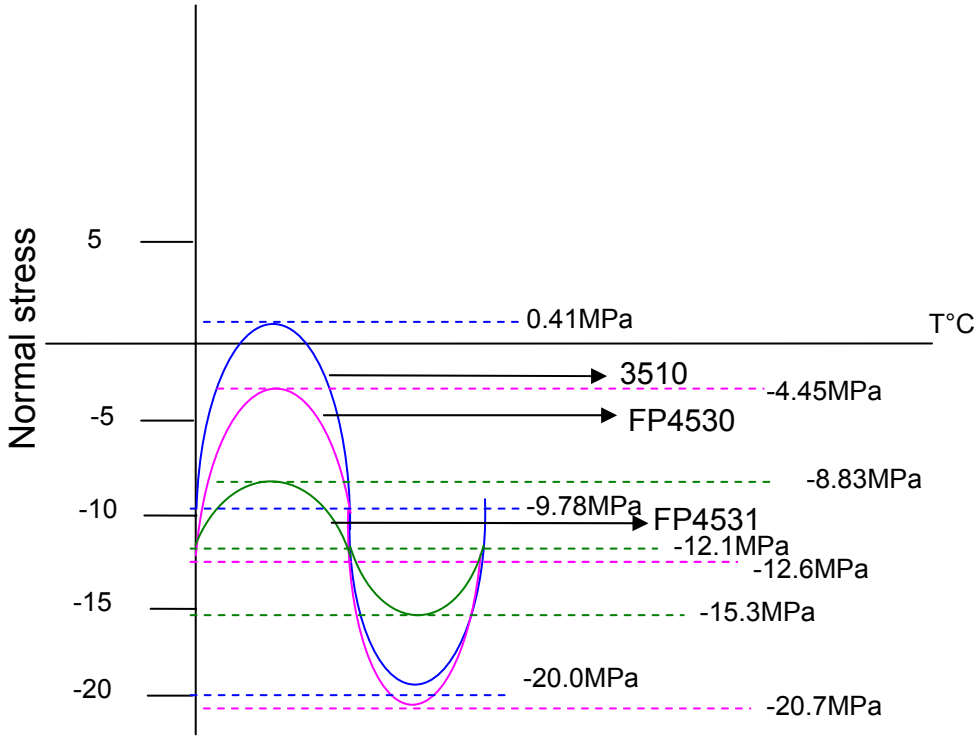

Figure 4.8 Schematic of sinusoidal plot of Mode I stresses for real underfill material properties.

4.3 Comparison of Mode I Cyclic Stress with Mode II Cyclic Stress

It is evident from section 4.2 that cyclic Mode I stresses should be considered in the development of a fatigue life for BGA interconnects. The development of a fatigue life model based on a fracture approach requires that crack of known size be embedded in the material under investigation and studied.

The following example provides a guideline for how researchers can determine the approximate loading (both Mode I and Mode II) to apply experimentally to the test specimen in the development of an appropriate fracture based fatigue life model. Consider a one inch by one inch BGA package for aerospace applications where the temperature is cycled from 5°C to 45°C. For simplicity a ten by ten array of solder interconnects is depicted in the Figure 4.9. The

difference in coefficient of thermal expansion of chip carrier and PCB is taken as $1.6x10^{-6}$/K. The stand off height of each joint is taken as 0.5mm and radius of the pad is 0.4mm. The solder interconnects in this BGA package are made of eutectic solder with E_s=32GPa and Poisson's ratio, υ_s=0.3 and are subjected to a thermal loading from 25°C to 5°C. According to equation (5), the Mode II shear stress, τ in the solder interconnects at a distance of L=18mm is 14.17MPa and at a distance of L=6mm is 4.72MPa.

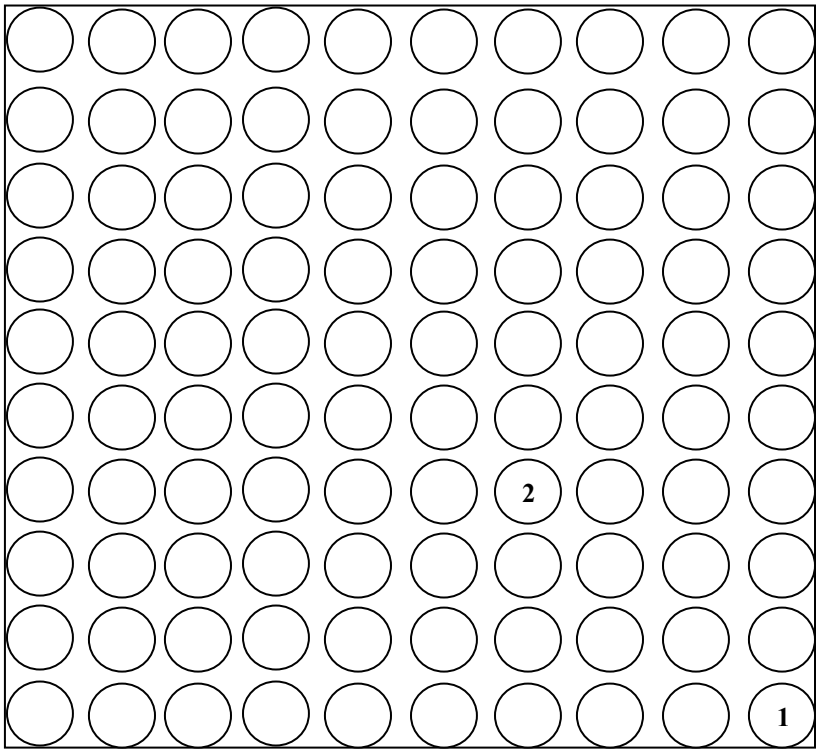

1: L=18mm τ = 14.17MPa
2: L=6mm τ = 4.72MPa

Figure 4.9 Schematic of top view of a ten by ten array of solder interconnects in BGA package (the numbered joints represents the joints for which shear stress is calculated).

Assume, for example, that the 3510 underfill is being considered and the fatigue life of the joint located at 6 mm from the center of the package is in question. During one thermal cycle, the shear stress arising from the mismatch in coefficient of thermal expansion between chip

carrier and the PCB fluctuates from +4.72MPa to -4.72MPa. The mode I normal stress fluctuates according to figure 4.8 from 0.4MPa to -20.0 MPa.

5. Conclusions and Recommendations

The influence of underfill on BGA package fatigue life has been investigated in this present research. With an increase in effort to reduce the size of electronic packages, much of the research has been motivated towards the reliability of solder joints in present day technology. A finite element model of unit cell geometry of a BGA package was developed using ANSYS 7.1 to analyze the significance of Mode I cyclic loading in the solder interconnects. It was proven that these Mode I cyclic stresses are significant and are of same order of magnitude when compared to Mode I steady state stresses obtained by Larson and Verges (2004).

Also the influence of underfill parameters such as E_u, υ_u, and α_u on Mode I cyclic stresses have been determined. It has been observed that as the coefficient of thermal expansion of underfill material increases, the amplitude of the normal cyclic stresses increases. For an increase in Poisson's ratio and stiffness of underfill material, the amplitude of the Mode I cyclic stresses also increases. However, it is evident that as the stiffness of the underfill material increases, v_u and α_u have a greater influence on the resulting normal stresses.

When adding the residual stresses induced in the solder upon curing of the underfill to the cyclic Mode I stresses caused by mismatch of solder and underfill properties during thermal cycling, a strong dependence on the coefficient of thermal expansion is observed. For a linear shrinkage of 0.6% of the underfill material, results indicate for all material combinations possessing a coefficient of thermal expansion, α_u, greater than around 70×10^{-6}/K, the solder will experience a tensile loading during thermal cycling that increases in magnitude with an increase

in E_u, ν_u, and α_u, and a decrease in *%sh*. Three popular underfills were also investigated in this study: FP4531, FP4530, and 3510. In comparing these three underfills, it is observed that during any one thermal cycle, use of the 3510 underfill would cause the solder to experience tension during a portion of the thermal cycling.

This work proves that more research is to be geared towards experimentally determining the fatigue life of fractured joints subjected to a combined Mode I and Mode II cyclic loading. It follows that such results would aide in the development of a fatigue life equation that incorporates a combined Mode I and Mode II cyclic loading.

References

1. Larson, M.C., Liu, X., and Verges, M. A., 2004, "Predicting Residual Stresses in Area Array Packages Induced by Underfill Shrinkage", submitted to the *Journal of Microelectronics Reliability*.

2. Larson, M. C. and Verges, M. A., 2003, "Extending the Fatigue Life of Solder Grid Array (SGA) Electronic Packages", *Journal of Electronic Packaging*, Vol.125, pp.18-23.

3. Ligi, Z., Li, W., Xiaoming, X., and Kempe, W., 2002, "An Investigation on Thermal Reliability of underfilled PBGA Solder Joints", *IEEE Transactions on Electronics Packaging Manufacturing,* vol-25, No.4, pp. 284-288.

4. Pyland, J., Pucha, R., and Sitaraman, S., 2001, "Effect of Underfill on BGA reliability", *Electronic Components and Technology Conference*, pp. 85-90.

5. Nemeth, N., Illetalvi-Vitez, Z., and Harsanyi, G., 2000, "Review of Reliability of Advanced Component Packaging Technologies", *2000 Proceedings: 50th Electronic Components Technology* Wednesday poster session, pp.1605-1609.

6. Wang, L., and Wong, C.P., 2000, "Recent advances in the underfill technology for Flipchip, Ball Grid Array and Chip Scale Package Applications", *International symposium on electronic materials and packaging*:Nov 30-Dec 2, Hong Kong, pp.224-231.

7. T.Burnette, Z.Johnson, T.Koschmieder, and W.Oyler, 2000, "underfilled BGA'S for ceramic bga packages and board level reliability", *2000 Proceedings: 50th Electronic Components & Technology Conference*, May 21-24, Las Vegas, Nevada, USA, pp.1221-1226.

8. S.C.Hung, P.J.Zheng, S.C.Lee, S.H.Ho, and H.N.Chen, 2000, "Thermal Cyclic Fatigue of Interconnect of a Flex type BGA", Electronic Components and Technology Conference, pp.1384-1391.

9. Kaga, Y., Yu, Q., Shiratori, M., 1999, "Thermal Fatigue Assessment for Solder Joints of Underfill Assembly", *Advances in Electronic Packaging*, Vol.26, pp.271-275.

10. C. Basaran, and R. Chandraroy, 1997 "Finite element simulation of the temperature cycling tests", *IEEE Transaction component hybrids and Manufacturing Technology* , Vol.20 , pp.530-536.

11. Verges, M. A., 1999, "An Investigation of Interconnect Geometry and Fatigue Life of Ball Grid Array Electronic Packages", Ph.D.thesis.

12. Bjorndahl, W.D., Selk, K., and Chen, W., 1997, "Surface Mount Technology Capabilities and Requirements", *IEEE Aerospace Conference Proceedings* ,Vol.4, pp.285-291.

13. Yao, D., Z. Zhang, and J.K.Shang, 1996, "An Experimental Technique for Studying Mixed-Mode Fatigue Crack Growth in Solder Joints", *Journal of Electronic Packaging*, Vol.118, pp. 45-48.

14. H.D.Solmon, E.D.Tolksdorf, 1995, "Energy Approach to the Fatigue of 60/40 Solder: Part I-Influence of Temperature and Cycle Frequency", *Journal of Electronic Packaging* , Vol.117, pp.130-135.

15. Pao, Y., 1992, "A Fracture Mechanics approach to thermal fatigue life prediction of joints", *IEEE transactions on components, hybrids, and manufacturing*, Vol.15, pp.559-570.

16. Vaynman, S., McKeown, S. A., 1991, "Energy based Methodology for the Fatigue–life prediction of Solder materials", *Electronic components and Technology Conference*, pp.671-676.

17. Frear, D., Morgan, H., Burchett, S., and Lau, J., 1994, *The Mechanics of Solder Alloy Interconnects*, Van Nostrand Reinhold Publications, New York.

18. Anderson T.L., IInd Edition, 1995, *Fracture Mechanics Fundamentals and Applications*, CRC Press, Boca Raton.

19. Lau, J., 1995, *Ball Grid Array Technology*, Mc-Graw Hill Publications, New York.

20. Hwang, Jennie, S., 1995, *Ball Grid Array & Fine Pitch Peripheral Interconnections A handbook of Technology and Applications*, Electro Chemical Publications.

Appendix A

```
FINISH
/CLEAR
/TITLE, Influence of underfill on BGA package fatigue life

/PREP7
ET, 1, PLANE182,,, 1          !element type plane182 with axisymmetric elements

DOF, UX, UY

! Section 3.3

MP, EX, 1,32E9                ! Young's modulus of solder material
MP, PRXY, 1, 0.3              ! Poison's ratio
MP, ALPX, 1, 24.1E-6          ! Coefficient of thermal expansion


MP, EX, 2, 5.0E9              ! Young's modulus of underfill material
MP, PRXY, 2, 0.2              ! Poison's ratio
MP, ALPX, 2, 10E-6            ! Coefficient of thermal expansion
TB, BISO, 1
TBDATA, 1,33E6                ! Yield stress (Pa)
TBDATA, 2, 0.01               ! Tangent modulus (Pa)

! Section 3.1

!creation of key points to generate the two rectangles

K, 1, 0, 0
K, 2, 0.0004, 0
K, 3, 0.0004, 0.00025
K, 4, 0, 0.00025
K, 5, 0.000635, 0
K, 6, 0.000635, 0.00025

!to create rectangular areas
```

```
A, 1, 2, 3, 4
A, 2, 3, 6, 5
AGLUE, ALL              ! To glue both the rectangles
```

! Section 3.5

```
! MESHING
MAT, 1
LESIZE, 1,,, 20
LESIZE, 2,,, 20
LESIZE, 3,,, 20
LESIZE, 4,,, 20
AMESH, 1

Mat, 2
LESIZE, 7,,, 20
LESIZE, 6,,, 20
LESIZE, 5,,, 20
AMESH, 2
```

! Section 3.2

```
! Constraint equations to implement the condition for top edge
! of the rectangle to move in uniform y-direction

CE, 1, 0, 42, UY, 1, 61, UY, -1,
J=2
*DO, I, 61, 44, -1
CE, J, 0, I, UY, 1, I-1, UY, -1,
J=J+1
*ENDDO
CE, 20, 0, 43, UY, 1, 22, UY, -1,
CE, 21, 0, 22, UY, 1, 443, UY, -1,
J=22
*DO, I, 443, 460, 1
CE, J, 0, I, UY, 1, I+1, UY, -1,
J=J+1
*ENDDO
CE, 40, 0, 461, UY, 1, 442, UY, -1,

! Boundary conditions
NSEL, S, LOC, Y, 0
D,ALL,UX
D, ALL, UY

NSEL, S, LOC, X, 0
```

```
D, ALL, UX

NSEL, S, LOC, Y, 0.00025
D, ALL, UX

NSEL, S, LOC, X, 0.000635
D, ALL, UX


TREF, 298   !reference temperature
ALLSEL
SAVE
FINI
```

! Section 3.4

```
/SOLUTION

SOLCONTROL, ON              ! Specifies whether to use optimized nonlinear
                            !solution defaults and some enhanced internal
                            !solution algorithms.
TIME, 1.0E-8
DELT, 1.0E-8, 1.0E-9, 1.0E-8   !specifies time step size to be used for load step
OUTRES, ALL, 100000            !controls the solution data written to the database
OUTPR, ALL, 100000             !controls the solution output

TUNIF, 298                  !uniform temperature
SOLVE
SAVE

DELT, 1.0E-6, 1.0E-6, 500000.0
OUTRES, ALL, ALL
OUTPR, ALL, LAST
BF, ALL, TEMP, 278           !uniform temperature reduction
SOLVE
SAVE
FINISH

! To display the solution
/POST1
PLNSOL, S, Y
FINISH
/EOF
```

Appendix B

Table B.1 The most tensile stresses induced in the solder during one thermal cycle when temperature is 5°C and E_u = 2.0GPa

% sh	α_u (1E-6/K)	σ_s (Pa)	σ_c (Pa)	$\sigma_s + \sigma_c$ (Pa)
0.2	10	-1.34E+06	3.17E+06	1.83E+06
0.2	40	-1.34E+06	1.60E+05	-1.18E+06
0.2	70	-1.34E+06	2.84E+06	1.51E+06
0.2	100	-1.34E+06	5.84E+06	4.51E+06
0.4	10	-2.67E+06	3.17E+06	4.98E+05
0.4	40	-2.67E+06	1.60E+05	-2.51E+06
0.4	70	-2.67E+06	2.84E+06	1.71E+05
0.4	100	-2.67E+06	5.84E+06	3.17E+06
0.6	10	-4.01E+06	3.17E+06	-8.38E+05
0.6	40	-4.01E+06	1.60E+05	-3.85E+06
0.6	70	-4.01E+06	2.84E+06	-1.16E+06
0.6	100	-4.01E+06	5.84E+06	1.84E+06
0.8	10	-5.34E+06	3.17E+06	-2.17E+06
0.8	40	-5.34E+06	1.60E+05	-5.18E+06
0.8	70	-5.34E+06	2.84E+06	-2.50E+06
0.8	100	-5.34E+06	5.84E+06	5.00E+05
1.0	10	-6.68E+06	3.17E+06	-3.51E+06
1.0	40	-6.68E+06	1.60E+05	-6.52E+06
1.0	70	-6.68E+06	2.84E+06	-3.84E+06
1.0	100	-6.68E+06	5.84E+06	-8.36E+05

(a)ν_u = 0.2

% sh	α_u (1E-6/K)	σ_s (Pa)	σ_c (Pa)	$\sigma_s + \sigma_c$ (Pa)
0.2	10	-1.53E+06	2.97E+06	1.45E+06
0.2	40	-1.53E+06	1.40E+06	-1.22E+05
0.2	70	-1.53E+06	5.78E+06	4.25E+06
0.2	100	-1.53E+06	1.01E+07	8.62E+06
0.4	10	-3.05E+06	2.97E+06	-7.86E+04
0.4	40	-3.05E+06	1.40E+06	-1.65E+06
0.4	70	-3.05E+06	5.78E+06	2.72E+06
0.4	100	-3.05E+06	1.01E+07	7.09E+06
0.6	10	-4.58E+06	2.97E+06	-1.61E+06
0.6	40	-4.58E+06	1.40E+06	-3.18E+06
0.6	70	-4.58E+06	5.78E+06	1.20E+06
0.6	100	-4.58E+06	1.01E+07	5.57E+06
0.8	10	-6.11E+06	2.97E+06	-3.13E+06
0.8	40	-6.11E+06	1.40E+06	-4.70E+06
0.8	70	-6.11E+06	5.78E+06	-3.31E+05
0.8	100	-6.11E+06	1.01E+07	4.04E+06
1.0	10	-7.63E+06	2.97E+06	-4.66E+06
1.0	40	-7.63E+06	1.40E+06	-6.23E+06
1.0	70	-7.63E+06	5.78E+06	-1.86E+06
1.0	100	-7.63E+06	1.01E+07	2.51E+06

(b)ν_u = 0.3

% sh	α_u (1E-6/K)	σ_s (Pa)	σ_c (Pa)	$\sigma_s + \sigma_c$ (Pa)
0.2	10	-1.78E+06	2.64E+06	8.54E+05
0.2	40	-1.78E+06	5.37E+06	3.59E+06
0.2	70	-1.78E+06	1.34E+07	1.16E+07
0.2	100	-1.78E+06	2.18E+07	2.00E+07
0.4	10	-3.56E+06	2.64E+06	-9.27E+05
0.4	40	-3.56E+06	5.37E+06	1.81E+06
0.4	70	-3.56E+06	1.34E+07	9.81E+06
0.4	100	-3.56E+06	2.18E+07	1.83E+07
0.6	10	-5.34E+06	2.64E+06	-2.71E+06
0.6	40	-5.34E+06	5.37E+06	2.48E+04
0.6	70	-5.34E+06	1.34E+07	8.03E+06
0.6	100	-5.34E+06	2.18E+07	1.65E+07
0.8	10	-7.12E+06	2.64E+06	-4.49E+06
0.8	40	-7.12E+06	5.37E+06	-1.76E+06
0.8	70	-7.12E+06	1.34E+07	6.25E+06
0.8	100	-7.12E+06	2.18E+07	1.47E+07
1.0	10	-8.91E+06	2.64E+06	-6.27E+06
1.0	40	-8.91E+06	5.37E+06	-3.54E+06
1.0	70	-8.91E+06	1.34E+07	4.46E+06
1.0	100	-8.91E+06	2.18E+07	1.29E+07

(c)ν_u = 0.4

Table B.2 The most tensile stresses induced in the solder during one thermal cycle when temperature is 5°C and E_u = 3.5 GPa

% sh	α_u (1E-6/K)	σ_s (Pa)	σ_c (Pa)	$\sigma_s + \sigma_c$ (Pa)
0.2	10	-2.22E+06	3.93E+06	1.71E+06
0.2	40	-2.22E+06	9.52E+05	-1.27E+06
0.2	70	-2.22E+06	5.82E+06	3.60E+06
0.2	100	-2.22E+06	1.07E+07	8.48E+06
0.4	10	-4.44E+06	3.93E+06	-5.15E+05
0.4	40	-4.44E+06	9.52E+05	-3.49E+06
0.4	70	-4.44E+06	5.82E+06	1.38E+06
0.4	100	-4.44E+06	1.07E+07	6.26E+06
0.6	10	-6.66E+06	3.93E+06	-2.74E+06
0.6	40	-6.66E+06	9.52E+05	-5.71E+06
0.6	70	-6.66E+06	5.82E+06	-8.38E+05
0.6	100	-6.66E+06	1.07E+07	4.03E+06
0.8	10	-8.88E+06	3.93E+06	-4.96E+06
0.8	40	-8.88E+06	9.52E+05	-7.93E+06
0.8	70	-8.88E+06	5.82E+06	-3.06E+06
0.8	100	-8.88E+06	1.07E+07	1.81E+06
1.0	10	-1.11E+07	3.93E+06	-7.18E+06
1.0	40	-1.11E+07	9.52E+05	-1.02E+07
1.0	70	-1.11E+07	5.82E+06	-5.28E+06
1.0	100	-1.11E+07	1.07E+07	-4.08E+05

(a) ν_u = 0.2

% sh	α_u (1E-6/K)	σ_s (Pa)	σ_c (Pa)	$\sigma_s + \sigma_c$ (Pa)
0.2	10	-2.54E+06	3.61E+06	1.08E+06
0.2	40	-2.54E+06	3.37E+06	8.28E+05
0.2	70	-2.54E+06	1.03E+07	7.80E+06
0.2	100	-2.54E+06	1.73E+07	1.48E+07
0.4	10	-5.08E+06	3.61E+06	-1.46E+06
0.4	40	-5.08E+06	3.37E+06	-1.71E+06
0.4	70	-5.08E+06	1.03E+07	5.27E+06
0.4	100	-5.08E+06	1.73E+07	1.22E+07
0.6	10	-7.61E+06	3.61E+06	-4.00E+06
0.6	40	-7.61E+06	3.37E+06	-4.25E+06
0.6	70	-7.61E+06	1.03E+07	2.73E+06
0.6	100	-7.61E+06	1.73E+07	9.70E+06
0.8	10	-1.02E+07	3.61E+06	-6.54E+06
0.8	40	-1.02E+07	3.37E+06	-6.79E+06
0.8	70	-1.02E+07	1.03E+07	1.89E+05
0.8	100	-1.02E+07	1.73E+07	7.16E+06
1.0	10	-1.27E+07	3.61E+06	-9.08E+06
1.0	40	-1.27E+07	3.37E+06	-9.33E+06
1.0	70	-1.27E+07	1.03E+07	-2.35E+06
1.0	100	-1.27E+07	1.73E+07	4.63E+06

(b) ν_u = 0.3

% sh	α_u (1E-6/K)	σ_s (Pa)	σ_c (Pa)	$\sigma_s + \sigma_c$ (Pa)
0.2	10	-2.96E+06	3.11E+06	1.44E+05
0.2	40	-2.96E+06	9.06E+06	6.10E+06
0.2	70	-2.96E+06	2.14E+07	1.84E+07
0.2	100	-2.96E+06	3.30E+07	3.00E+07
0.4	10	-5.92E+06	3.11E+06	-2.82E+06
0.4	40	-5.92E+06	9.06E+06	3.14E+06
0.4	70	-5.92E+06	2.14E+07	1.55E+07
0.4	100	-5.92E+06	3.30E+07	2.70E+07
0.6	10	-8.88E+06	3.11E+06	-5.78E+06
0.6	40	-8.88E+06	9.06E+06	1.80E+05
0.6	70	-8.88E+06	2.14E+07	1.25E+07
0.6	100	-8.88E+06	3.30E+07	2.41E+07
0.8	10	-1.18E+07	3.11E+06	-8.74E+06
0.8	40	-1.18E+07	9.06E+06	-2.78E+06
0.8	70	-1.18E+07	2.14E+07	9.55E+06
0.8	100	-1.18E+07	3.30E+07	2.11E+07
1.0	10	-1.48E+07	3.11E+06	-1.17E+07
1.0	40	-1.48E+07	9.06E+06	-5.74E+06
1.0	70	-1.48E+07	2.14E+07	6.59E+06
1.0	100	-1.48E+07	3.30E+07	1.82E+07

(c) ν_u = 0.4

Table B.3 The most tensile stresses induced in the solder during one thermal cycle when temperature is 5°C and E_u = 5.0GPa

% sh	α_u (1E-6/K)	σ_s (Pa)	σ_c (Pa)	$\sigma_s + \sigma_c$(Pa)
0.2	10	-3.01E+06	4.65E+06	1.64E+06
0.2	40	-3.01E+06	1.85E+06	-1.15E+06
0.2	70	-3.01E+06	8.35E+06	5.35E+06
0.2	100	-3.01E+06	1.48E+07	1.18E+07
0.4	10	-6.01E+06	4.65E+06	-1.36E+06
0.4	40	-6.01E+06	1.85E+06	-4.16E+06
0.4	70	-6.01E+06	8.35E+06	2.34E+06
0.4	100	-6.01E+06	1.48E+07	8.84E+06
0.6	10	-9.02E+06	4.65E+06	-4.37E+06
0.6	40	-9.02E+06	1.85E+06	-7.16E+06
0.6	70	-9.02E+06	8.35E+06	-6.66E+05
0.6	100	-9.02E+06	1.48E+07	5.83E+06
0.8	10	-1.20E+07	4.65E+06	-7.37E+06
0.8	40	-1.20E+07	1.85E+06	-1.02E+07
0.8	70	-1.20E+07	8.35E+06	-3.67E+06
0.8	100	-1.20E+07	1.48E+07	2.83E+06
1.0	10	-1.50E+07	4.65E+06	-1.04E+07
1.0	40	-1.50E+07	1.85E+06	-1.32E+07
1.0	70	-1.50E+07	8.35E+06	-6.68E+06
1.0	100	-1.50E+07	1.48E+07	-1.79E+05

(a)ν_u = 0.2

% sh	α_u (1E-6/K)	σ_s (Pa)	σ_c (Pa)	$\sigma_s + \sigma_c$ (Pa)
0.2	10	-3.44E+06	4.23E+06	7.97E+05
0.2	40	-3.44E+06	4.94E+06	1.50E+06
0.2	70	-3.44E+06	1.41E+07	1.07E+07
0.2	100	-3.44E+06	2.39E+07	2.04E+07
0.4	10	-6.87E+06	4.23E+06	-2.64E+06
0.4	40	-6.87E+06	4.94E+06	-1.93E+06
0.4	70	-6.87E+06	1.41E+07	7.23E+06
0.4	100	-6.87E+06	2.39E+07	1.70E+07
0.6	10	-1.03E+07	4.23E+06	-6.07E+06
0.6	40	-1.03E+07	4.94E+06	-5.37E+06
0.6	70	-1.03E+07	1.41E+07	3.80E+06
0.6	100	-1.03E+07	2.39E+07	1.36E+07
0.8	10	-1.37E+07	4.23E+06	-9.51E+06
0.8	40	-1.37E+07	4.94E+06	-8.80E+06
0.8	70	-1.37E+07	1.41E+07	3.64E+05
0.8	100	-1.37E+07	2.39E+07	1.01E+07
1.0	10	-1.72E+07	4.23E+06	-1.29E+07
1.0	40	-1.72E+07	4.94E+06	-1.22E+07
1.0	70	-1.72E+07	1.41E+07	-3.07E+06
1.0	100	-1.72E+07	2.39E+07	6.71E+06

(b)ν_u = 0.3

% sh	α_u (1E-6/K)	σ_s (Pa)	σ_c(Pa)	$\sigma_s + \sigma_c$ (Pa)
0.2	10	-4.01E+06	3.59E+06	-4.14E+05
0.2	40	-4.01E+06	1.18E+07	7.80E+06
0.2	70	-4.01E+06	2.64E+07	2.24E+07
0.2	100	-4.01E+06	3.78E+07	3.38E+07
0.4	10	-8.02E+06	3.59E+06	-4.42E+06
0.4	40	-8.02E+06	1.18E+07	3.79E+06
0.4	70	-8.02E+06	2.64E+07	1.84E+07
0.4	100	-8.02E+06	3.78E+07	2.98E+07
0.6	10	-1.20E+07	3.59E+06	-8.43E+06
0.6	40	-1.20E+07	1.18E+07	-2.20E+05
0.6	70	-1.20E+07	2.64E+07	1.44E+07
0.6	100	-1.20E+07	3.78E+07	2.58E+07
0.8	10	-1.60E+07	3.59E+06	-1.24E+07
0.8	40	-1.60E+07	1.18E+07	-4.23E+06
0.8	70	-1.60E+07	2.64E+07	1.04E+07
0.8	100	-1.60E+07	3.78E+07	2.18E+07
1.0	10	-2.00E+07	3.59E+06	-1.64E+07
1.0	40	-2.00E+07	1.18E+07	-8.23E+06
1.0	70	-2.00E+07	2.64E+07	6.38E+06
1.0	100	-2.00E+07	3.78E+07	1.78E+07

(c)ν_u = 0.4

Table B.4 The most tensile stresses induced in the solder during one thermal cycle when temperature is 5°C and E_u = 6.5 GPa

% sh	α_u (1E-6/K)	σ_s (Pa)	σ_c (Pa)	$\sigma_s + \sigma_c$ (Pa)
0.2	10	-3.69E+06	5.33E+06	1.64E+06
0.2	40	-3.69E+06	2.59E+06	-1.10E+06
0.2	70	-3.69E+06	1.05E+07	6.83E+06
0.2	100	-3.69E+06	1.89E+07	1.53E+07
0.4	10	-7.38E+06	5.33E+06	-2.05E+06
0.4	40	-7.38E+06	2.59E+06	-4.79E+06
0.4	70	-7.38E+06	1.05E+07	3.14E+06
0.4	100	-7.38E+06	1.89E+07	1.16E+07
0.6	10	-1.11E+07	5.33E+06	-5.74E+06
0.6	40	-1.11E+07	2.59E+06	-8.48E+06
0.6	70	-1.11E+07	1.05E+07	-5.53E+05
0.6	100	-1.11E+07	1.89E+07	7.87E+06
0.8	10	-1.48E+07	5.33E+06	-9.43E+06
0.8	40	-1.48E+07	2.59E+06	-1.22E+07
0.8	70	-1.48E+07	1.05E+07	-4.24E+06
0.8	100	-1.48E+07	1.89E+07	4.18E+06
1.0	10	-1.85E+07	5.33E+06	-1.31E+07
1.0	40	-1.85E+07	2.59E+06	-1.59E+07
1.0	70	-1.85E+07	1.05E+07	-7.93E+06
1.0	100	-1.85E+07	1.89E+07	4.91E+05

(a)ν_u = 0.2

% sh	α_u (1E-6/K)	σ_s (Pa)	σ_c (Pa)	$\sigma_s + \sigma_c$ (Pa)
0.2	10	-4.22E+06	4.83E+06	6.11E+05
0.2	40	-4.22E+06	6.22E+06	2.00E+06
0.2	70	-4.22E+06	1.74E+07	1.32E+07
0.2	100	-4.22E+06	2.83E+07	2.41E+07
0.4	10	-8.43E+06	4.83E+06	-3.61E+06
0.4	40	-8.43E+06	6.22E+06	-2.22E+06
0.4	70	-8.43E+06	1.74E+07	8.94E+06
0.4	100	-8.43E+06	2.83E+07	1.99E+07
0.6	10	-1.27E+07	4.83E+06	-7.82E+06
0.6	40	-1.27E+07	6.22E+06	-6.44E+06
0.6	70	-1.27E+07	1.74E+07	4.72E+06
0.6	100	-1.27E+07	2.83E+07	1.56E+07
0.8	10	-1.69E+07	4.83E+06	-1.20E+07
0.8	40	-1.69E+07	6.22E+06	-1.07E+07
0.8	70	-1.69E+07	1.74E+07	5.05E+05
0.8	100	-1.69E+07	2.83E+07	1.14E+07
1.0	10	-2.11E+07	4.83E+06	-1.63E+07
1.0	40	-2.11E+07	6.22E+06	-1.49E+07
1.0	70	-2.11E+07	1.74E+07	-3.71E+06
1.0	100	-2.11E+07	2.83E+07	7.21E+06

(b)ν_u = 0.3

% sh	α_u (1E-6/K)	σ_s (Pa)	σ_c (Pa)	$\sigma_s + \sigma_c$ (Pa)
0.2	10	-4.92E+06	4.08E+06	-8.41E+05
0.2	40	-4.92E+06	1.39E+07	8.98E+06
0.2	70	-4.92E+06	2.94E+07	2.45E+07
0.2	100	-4.92E+06	4.05E+07	3.56E+07
0.4	10	-9.84E+06	4.08E+06	-5.76E+06
0.4	40	-9.84E+06	1.39E+07	4.06E+06
0.4	70	-9.84E+06	2.94E+07	1.95E+07
0.4	100	-9.84E+06	4.05E+07	3.06E+07
0.6	10	-1.48E+07	4.08E+06	-1.07E+07
0.6	40	-1.48E+07	1.39E+07	-8.57E+05
0.6	70	-1.48E+07	2.94E+07	1.46E+07
0.6	100	-1.48E+07	4.05E+07	2.57E+07
0.8	10	-1.97E+07	4.08E+06	-1.56E+07
0.8	40	-1.97E+07	1.39E+07	-5.78E+06
0.8	70	-1.97E+07	2.94E+07	9.70E+06
0.8	100	-1.97E+07	4.05E+07	2.08E+07
1.0	10	-2.46E+07	4.08E+06	-2.05E+07
1.0	40	-2.46E+07	1.39E+07	-1.07E+07
1.0	70	-2.46E+07	2.94E+07	4.78E+06
1.0	100	-2.46E+07	4.05E+07	1.59E+07

(c)ν_u = 0.4

Table B.5 The most tensile stresses induced in the solder during one thermal cycle when temperature is 5°C and E_u =8.0 GPa

% sh	α_u (1E-6/K)	σ_s (Pa)	σ_c (Pa)	$\sigma_s + \sigma_c$ (Pa)
0.2	10	-4.27E+06	5.99E+06	1.71E+06
0.2	40	-4.27E+06	3.21E+06	-1.07E+06
0.2	70	-4.27E+06	1.24E+07	8.12E+06
0.2	100	-4.27E+06	2.21E+07	1.79E+07
0.4	10	-8.55E+06	5.99E+06	-2.56E+06
0.4	40	-8.55E+06	3.21E+06	-5.34E+06
0.4	70	-8.55E+06	1.24E+07	3.85E+06
0.4	100	-8.55E+06	2.21E+07	1.36E+07
0.6	10	-1.28E+07	5.99E+06	-6.84E+06
0.6	40	-1.28E+07	3.21E+06	-9.62E+06
0.6	70	-1.28E+07	1.24E+07	-4.27E+05
0.6	100	-1.28E+07	2.21E+07	9.32E+06
0.8	10	-1.71E+07	5.99E+06	-1.11E+07
0.8	40	-1.71E+07	3.21E+06	-1.39E+07
0.8	70	-1.71E+07	1.24E+07	-4.70E+06
0.8	100	-1.71E+07	2.21E+07	5.05E+06
1.0	10	-2.14E+07	5.99E+06	-1.54E+07
1.0	40	-2.14E+07	3.21E+06	-1.82E+07
1.0	70	-2.14E+07	1.24E+07	-8.98E+06
1.0	100	-2.14E+07	2.21E+07	7.73E+05

(a) $\nu_u = 0.2$

% sh	α_u (1E-6/K)	σ_s (Pa)	σ_c (Pa)	$\sigma_s + \sigma_c$ (Pa)
0.2	10	-4.89E+06	5.40E+06	5.12E+05
0.2	40	-4.89E+06	7.27E+06	2.39E+06
0.2	70	-4.89E+06	2.02E+07	1.54E+07
0.2	100	-4.89E+06	3.12E+07	2.64E+07
0.4	10	-9.77E+06	5.40E+06	-4.37E+06
0.4	40	-9.77E+06	7.27E+06	-2.50E+06
0.4	70	-9.77E+06	2.02E+07	1.05E+07
0.4	100	-9.77E+06	3.12E+07	2.15E+07
0.6	10	-1.47E+07	5.40E+06	-9.26E+06
0.6	40	-1.47E+07	7.27E+06	-7.38E+06
0.6	70	-1.47E+07	2.02E+07	5.59E+06
0.6	100	-1.47E+07	3.12E+07	1.66E+07
0.8	10	-1.95E+07	5.40E+06	-1.41E+07
0.8	40	-1.95E+07	7.27E+06	-1.23E+07
0.8	70	-1.95E+07	2.02E+07	7.07E+05
0.8	100	-1.95E+07	3.12E+07	1.17E+07
1.0	10	-2.44E+07	5.40E+06	-1.90E+07
1.0	40	-2.44E+07	7.27E+06	-1.72E+07
1.0	70	-2.44E+07	2.02E+07	-4.18E+06
1.0	100	-2.44E+07	3.12E+07	6.81E+06

(b) $\nu_u = 0.3$

% sh	α_u (1E-6/K)	σ_s (Pa)	σ_c (Pa)	$\sigma_s + \sigma_c$ (Pa)
0.2	10	-5.70E+06	4.56E+06	-1.14E+06
0.2	40	-5.70E+06	1.56E+07	9.86E+06
0.2	70	-5.70E+06	3.13E+07	2.56E+07
0.2	100	-5.70E+06	4.22E+07	3.65E+07
0.4	10	-1.14E+07	4.56E+06	-6.84E+06
0.4	40	-1.14E+07	1.56E+07	4.16E+06
0.4	70	-1.14E+07	3.13E+07	1.99E+07
0.4	100	-1.14E+07	4.22E+07	3.08E+07
0.6	10	-1.71E+07	4.56E+06	-1.25E+07
0.6	40	-1.71E+07	1.56E+07	-1.54E+06
0.6	70	-1.71E+07	3.13E+07	1.42E+07
0.6	100	-1.71E+07	4.22E+07	2.51E+07
0.8	10	-2.28E+07	4.56E+06	-1.82E+07
0.8	40	-2.28E+07	1.56E+07	-7.24E+06
0.8	70	-2.28E+07	3.13E+07	8.46E+06
0.8	100	-2.28E+07	4.22E+07	1.94E+07
1.0	10	-2.85E+07	4.56E+06	-2.39E+07
1.0	40	-2.85E+07	1.56E+07	-1.29E+07
1.0	70	-2.85E+07	3.13E+07	2.76E+06
1.0	100	-2.85E+07	4.22E+07	1.37E+07

(c) $\nu_u = 0.4$

Vita

Geetha Chilakamarthi was born in Visakhapatnam, India. She received her Bachelor's degree in Mechanical Engineering from Jawaharlal Nehru Technological University, India. Then she enrolled in Master's program at University of New Orleans, LA and worked as a research assistant for Dr. Melody Verges. She graduated with a Master's degree in Mechanical Engineering in May 2004.